Modelling and Simulation of Deformation Localization in Fibrous Extracellular Matrix induced by Contractile Fibroblasts

By

CHRYSOVALANTOU KALAITZIDOU

Thesis Supervisor: Prof. PHOEBUS ROSAKIS

School of Medicine
UNIVERSITY OF CRETE

The work has been supported by the Institute of Applied & Computational Mathematics (IACM), Foundation for Research and Technology - Hellas (FORTH).

JANUARY 2019

Μοντελοποίηση και προσομοίωση των παραμορφώσεων στον Extracellular Matrix που εισάγονται από κύτταρα που συστέλλονται

ΧΡΥΣΟΒΑΛΑΝΤΟΥ ΚΑΛΑΪΤΖΙΔΟΥ

Επιβλέπων: Καθ. ΦΟΙΒΟΣ ΡΟΖΑΚΗΣ

ΙΑΤΡΙΚΗ ΣΧΟΛΗ

ΠΑΝΕΠΙΣΤΗΜΙΟ ΚΡΗΤΗΣ

Abstract

Living tissues are not just collections of packed cells. Much of a tissue's capacity consists of extracellular space which is largely filled by a complex meshwork, the Extracellular Matrix (ECM). Many cells bind to components of the extracellular matrix, which are mainly fibrous proteins (fibers). This cell-to-ECM adhesion is regulated by specific cell-surface cellular adhesion molecules. When cells contract, i.e. reduce their volume, they exert loads on the fibers and thereby deforming the Extracellular Matrix. The displacement or stress fields, that these deformations result in, serve as signals to other cells. As a respond to these signals, neighboring cells can detect and even approach each other. This mechanical property of a cell's microenvironment is essential for many of its processes, including cell division, differentiation, migration and morphogenesis.

In the current study, we implement a two dimensional discrete model of a fiber network to capture localized deformations induced by one or two contracting cells. We develop a constitutive model, for which the stored energy function of the network is formulated by starting from a nonlinear stress-stretch relation of a single fiber. We minimize the network's total energy and investigate the resulting deformations which support predictions from previously conducted experiments, including the long-range propagation of displacements induced by one contractile cell and the formation of tether-like bands between two contractile cells, mechanisms that have been associated with a number of essential cellular functions.

ΣΥΝΟΨΗ

Οι οργανικοί ιστοί δεν είναι απλά οργανωμένες ομάδες κυττάρων. Το μεγαλύτερό τους μέρος αποτελείται από ένα σύνθετο και πολύπλοκο εξωκυττάριο περιβάλλον, γνωστό ως *Extracellular Matrix* (ECM). Τα κύτταρα προσδένονται σε δομικά στοιχεία του ECM, τα οποία περιλαμβάνουν, ως επί το πλείστον, ινώδεις πρωτεΐνες που ονομάζονται *fibers*. Η πρόσδεση των κυττάρων ρυθμίζεται από ειδικά μόρια που βρίσκονται στην επιφάνειά τους και μέσω αυτής τα κύτταρα προκαλούν παραμορφώσεις στο περιβάλλον γύρω τους. Συγκεκριμένα, έχει παρατηρηθεί ότι καθώς συρρικνώνονται ασκούν δυνάμεις στους fibers με τους οποίους είναι προσδεδεμένα και έτσι αυτοί, με τη σείρα τους, παραμορφώνονται. Οι παραμορφώσεις αυτές λειτουργούν ως σήματα σε γειτονικά κύτταρα μέσω των οποίων τα κύτταρα επικοινωνούν και μερικές φορές πλησιάζουν μεταξύ τους. Αυτή η μηχανική ιδιότητα που διέπει το περιβάλλον του κυττάρου είναι πολύ σημαντική για πολλές από τις λειτουργίες του, όπως η κυτταρική διαίρεση, ο πολλαπλασιασμός και η μορφογένεση.

Σε αυτήν την έρευνα, υλοποιούμε ένα διδιάστατο διακριτό μοντέλο του ECM και μελετάμε τις μηχανικές ιδιότητες που τόν διέπουν και διευκολύνουν τις παραμορφώσεις που εισάγουν ένα ή δύο κύτταρα που συρρικνώνονται.

ACKNOWLEDGEMENTS

The current report contains the formulation of the project on which I worked during my master thesis. It has been a period of intense learning for me, not only in the scientific arena, but also on a personal level. I wish to reflect on the people who have supported and helped me throughout this time.

I would like to express my sincere gratitude towards my supervisor Prof. Phoebus Rosakis who entrusted me with this fascinating project, even if it was initially unfamiliar to me. His continuous support and guidance but, most of all, his patience have been the stepping stone that kept me on track, especially at times when I thought that I was not able to keep up. It is difficult to express how much grateful I am for being a member of his team.

Furthermore, I would also like to acknowledge Giorgos Grekas for his invaluable contribution to this work. For all these hours he spent discussing aspects of the problem and the code, talking about results and exchanging ideas, for the bafflement under which we kept debugging, a thank you is the least that I can say.

The journey towards this degree has been *dark and full of terrors** and one's company to deal with these terrors was essential. First of all, I owe a lot to my dearest colleagues Dimitris and Zacharias, for being there during almost everything. Thank you for your patience. I would also like to express my gratitude to Iordanis for his help and support, since the very beginning of my scientific career. Thank you for standing by my side.

However, there are certain people behind each page of this report, as well as behind every step that I take - my family. In this case, there are no words to reflect any thankfulness. Your trust empowered me while your sacrifices have brought me up to here. I want you to know that I tried to do my best out of it. I still do.

*George R.R.Martin, *A Song of Ice and Fire*

The present is theirs; the future, for which I really worked, is mine

— Nicola Tesla

AUTHOR'S DECLARATION

A dissertation was submitted to the School of Medicine, at the University of Crete, in accordance with the requirements of the Masters' of Science degree in *Bioinformatics*.

AUTHOR:
CHRYSOVALANTOU KALAITZIDOU

ASSESSMENT COMMITTEE:
PROF. PHOEBUS ROSAKIS (Supervisor)
DR. PANAYIOTA POIRAZI, DR. PAVLOS PAVLIDIS

TABLE OF CONTENTS

Page

CHAPTER 1

INTRODUCTION

This chapter introduces the basic biological concepts, beginning with the main structure, the Extracellular Matrix. We then continue with reporting the mechanical properties the matrix exhibits and have been found to regulate important cellular functions. At the last part of this section, we present the core of the model that is proposed in this study and how is that different from previous models.

1.1 The Extracellular Matrix

Cellular fate processes are regulated by intracellular signaling pathways and by the extracellular space that surrounds a cell, referred to as the *cell microenvironment*. Numerous studies have revealed that variations in the cellular microenvironment occurred due to chemical, biophysical, and topographical signals module important cell functions such as movement, shape and adhesion [13, 22]. Cells are continually faced with the complex tasks of sensing these inputs, processing the signals through signal transduction and gene regulation networks. Though, each cell is not only controlled by their microenvironment but they also induce changes and modifications to it, at the same time. These modifications are the result of the proximity and behavior of neighboring cells that favor cell-cell contact, as well as the chemistry and mechanics of the major component of a cell's microenvironment, the extracellular matrix, .

The **extracellular matrix (ECM)** is a highly active entity that is of vital importance serving as a critical regulator of developmental dynamics. In addition to providing structural support for the cells embedded within a tissue, the ECM determines and controls some of the most fundamental behaviors and characteristics of cells such as proliferation, adhesion, migration, polarity, differentiation, and apoptosis.

The ECM is a convoluted network composed of an array of macromolecules that link together to form a structurally stable compound, contributing to the mechanical properties of tissues. Major components include proteoglycans, cell-binding glycoproteins, as well as elastin and collagen fibers. Collagen is the most abundant fibrous protein within the ECM and constitutes up to 30% of the total protein mass of a multicellular animal [2].

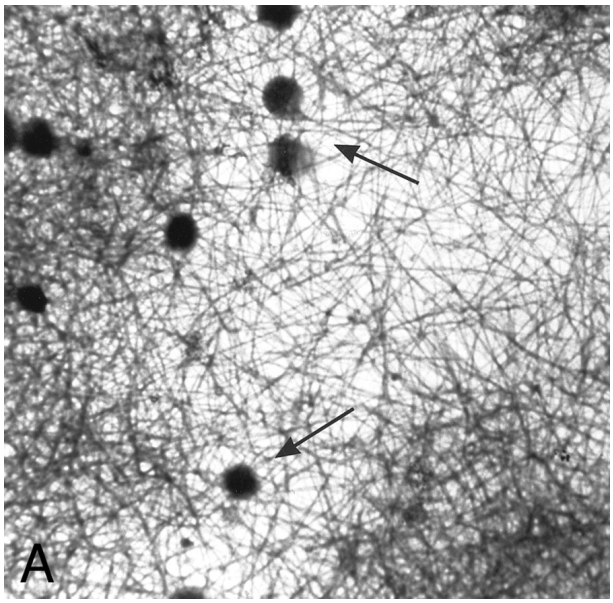

FIGURE 1.1. The Extracellular Matrix

At the scale of tissues, the ECM provides mechanical support that resists forces and provides structure. Being the main structural element of the ECM, the fibrous collagen networks provide tensile strength, regulate cell adhesion and direct tissue development [36]. At the cellular level, cells are attached to matrix fibers through *integrins*, Fig. (1.2), a family of cell-adhesion molecules. This binding of ECM proteins to cell surface integrins facilitates a significant influence on cell behaviors; it serves as the physical linkage between intracellular and extracellular compartments which mediates adhesion, resists mechanical stress and establishes a bi-directional mode of cell-matrix interaction [27].

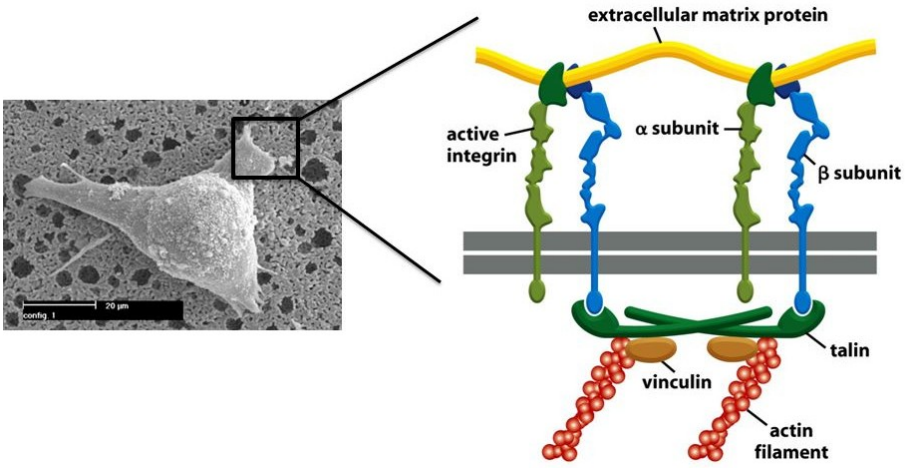

FIGURE 1.2. Cell - matrix binding through *integrins*

1.2 Mechanosensing

Cells sense biochemical and biophysical cues of their microenvironment and respond accordingly. These cues include, among others, *mechanical signals* that originate in the external cell environment or they can be signals from neighbouring cells transmitted through the ECM. ***Mechanosensing*** refers to the ability of cells to **sense** the mechanical state of the extracellular matrix. Consequently, the cells translate these signals into biochemical responses, a mechanism commonly known as *mechanotransduction* [35], that regulate critical cellular functions. For instance, the stiffness of the ECM in [9] was able to determine cell differentiation of mesenchymal stem cells. When these cells were cultured in gels of varying stiffness, they were directed in a specific lineage depending on how closely the gel resembled the mechanical stiffness of the respective *in vivo* tissue of the resulting cell type. Extracellular matrix stiffness, in addition, enables cells to generate forces whih in turn induce deformations in their surrounding space so that a specific cellular function is driven. In epithelial sheets, cells contract their cytoskeleton and in turn pulling forces are exerted on the extracellular components, leading to formation of tubes [19, 28]. Pulling forces are also induced by mesenchymal cells to their extracellular matrix which are transmitted to the epithelium and result in its remodelling [14]. Substrate rigidity and mechanical forces guide cell migration as well. Cells have the ability to respond to matrix rigidity by exerting contractile forces to deform their environment and use these deformations as preferable directions of their movement [20].
It is of vital importance to explore and understand the mechanical properties of the ECM that contribute in promoting a desirable cell phenotype or function. Equally prominent is to investigate its structural features and how these are being deformed due to traction fields induced by cells. These aspects together will help us understand how cells remodel their surrounding space in order to drive a specific function, which in some cases refers to a disease development.

The transmission of cell-induced forces has been demonstrated to be a result of the ***nonlinear*** elastic nature of the extracellular network. Many studies have contributed to this realization. For instance, in [37] contractile fibroblasts and human mesenchymal stem cells could achieve possible spreading by inducing locally stiffening in the fibrin gels they were embedded. This mechanism allowed them to mechanically interact with other cells with distance up to 5 cell lengths from their periphery. This long distant transmission of forces between cells is a process commonly observed in *in vivo* tissues. Remarkably, this effect was not detected on experiments held with linear elastic substrates. In another study [24], a long-range transmission of loads was detected when contractile fibroblasts were seeded in a nonlinear elastic fibrin matrix. The induced displacements propagated significantly further than those generated when linear elastic gel was used instead.
In the following section, we demonstrate a significant nonlinear property that fibrous biological materials such as ECM exhibit, which constitutes the basic feature of our model.

1.3 Nonlinear elasticity of ECM

The mechanical attributes of biological tissues are essential to their function and cannot be easily duplicated by synthetic materials. The mechanical relation between cells and their surrounding components has primarily been investigated using synthetic, linearly elastic materials. However, extracellular matrices are made up by networks of semiflexible biopolymers whose mechanics has been extensively studied and revealed their nonlinear elastic behavior [3, 6, 8, 15, 17]. Natural fibrous matrices stiffen as they are being increasingly deformed, in order to prevent deformations that could threaten the structural integrity of a tissue. However, these studies verified that fibrous matrices exhibit lower stiffness in compression than in tension. The property of increasing stiffness with increasing deformation is called ***strain stiffening*** and is one of the most important mechanical aspects of fibrous matrices [31, 36]. This nonlinear function that governs the extracellular matrix is originated in the mechanical behaviour of the individual fibers that these networks are composed of. In particular, it has been verified that filaments in these networks exhibit higher stiffness in tension than in compression. This means that they become stiffer when a tensile load would try to stretch them, but being subjected to a compressive load they would not show resistance [15, 31, 32]. Indeed, fibers exhibit very low resistance to bending, behaving similarly to a common string under compression. A string, when one pulls its two ends it resists tension. But if one pushes its ends towards each other, the string bends without resisting against its compression. This phenomenon refers to the ***buckling*** of fibers. In the image on the left, reproduced by [18], we see an example of fiber buckling. The blue boxes highlight an individual fiber undergoing a progressive buckling due to different compressive strains applied in the network. As the degree of network compression increases, the individual fiber appears increasingly bent.

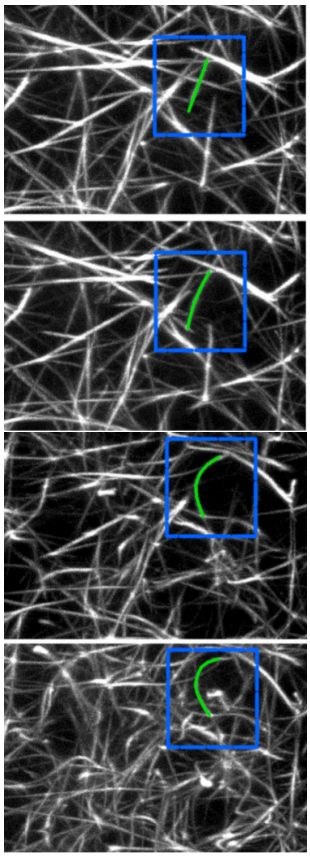

Upon buckling, fibers exhibit compliance, i.e. they become more flexible. As a result of this, the elasticity of the network gradually decreases with compression. Thereby, buckling of individual fibers can change the mechanical response of their network. Extracellular matrices exhibit larger stiffness in tension than compression because individual fibers buckle under compressive loads [6, 8, 17, 18, 32].

1.4 Cell-Cell communication

The transmission of forces generated by a cell over relatively long distances demonstrates a remarkable observation in fibrous extracellular matrices and has been proposed as a mechanism which enables cells to communicate with each other, as they sense and respond to mechanical signals sent by other cells. This communication takes place in multicellular structures where cells form long collagen lines of aligned fibers through the localized deformations they induce.

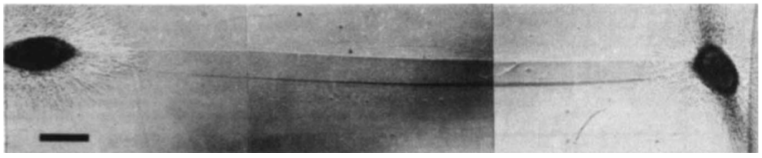

FIGURE 1.3. Fiber Alignment, reproduced by Harris *et al.,* 1981 [12] The first study to demonstrate that forces exerted by two tissue explants, embedded in a collagen gel, stretched and aligned the fibers between them, thereby forming inter-cellular *bands*.

The formation of fiber alignment constitutes a mechanical phenomenon that reflects the fundamental nonlinear properties of fibrous biological networks [29, 34]. It has been associated with a number of biological processes; isolated cells can create far-reaching mechanical gradients in order to achieve a pattern formation during wound-healing or tissue development [37], while interconnection of cells through fiber alignment coordinates cancer invasion and migration [7, 25, 29].

The question that arises is how the alignment of fibers between cells is associated with cell-cell communication. Notbohm and colleagues in [23] carried out experiments with pairs of contracting cells and reported the formation of tether-like bands of aligned and densely packed fibers connecting the cells, which were separated by a distance with order of 10 cell diameters. The cells *grew protrusions* along these tethers and across each other, Fig. (1.4); this phenomenon reflects why the formation of these bands is important for cell communication. Thereby it is essential to identify what mechanical properties the ECM should have in order to facilitate the formation of tethers that enable cells to communicate.

In order to understand the underline mechanisms of cell-cell communication through the fiber alignment, it is important to first investigate the decay of displacements induced by cells in a fiber network. The great distance of 10 cell diameters separating the cells in Notbohm's experiments

indicate that displacements each cell induced propagated over a long-range far from its boundary.

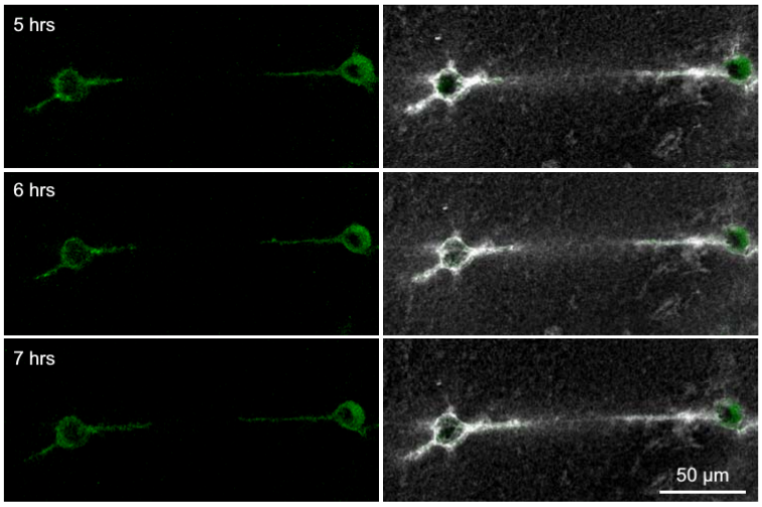

FIGURE 1.4. Notbohm *et al.,* 2015 [23]. Pairs of cells (green) spread toward one another along tethers. The cells apply tensile force to the fibrous matrix resulting in matrix tethers connecting the cells (white). These tethers have a high density of matrix fibres, as apparent by the bright fluorescent signal in the space between the cells. The cells then spread along these tethers. Times are hours after the cells were seeded in the matrix.

They investigated this long-range propagation of displacements in experiments held with isolated cells and reported significant findings: displacements induced by isolated cells, which were embedded in a three-dimensional fibrous matrix, travelled considerably further than displacements induced when cells were seeded in a linear elastic material. Furthermore, they indicated that these displacements would *decay slower with distance form the cell than predicted in a homogeneous linear elastic material*. They attributed these phenomena to the fact that fibers lose stiffness in compression particularly is due to buckling of individual fibers in compression.
To validate this hypothesis, they developed a finite-element based model and investigated two cases. In first case, elements of the model represented individual fibers, exhibiting a bilinear force-strain* relation (Fig. 1.5a, solid blue line), with a smaller slope in compression than in tension. Note that the slope in a stress-strain curve represents the *stiffness* of an element. Thus, the smaller slope corresponds to lower stiffness upon strains lower than zero, i.e. fibers are under a compressive load, and the bigger slope corresponds to higher stiffness upon positive strains, for fibers subjected to a tensile load. In second case (Fig. 1.5b, solid red line) the stiffness increased with strain in tension, so that stiffness increases with strain, modeling buckling combined with tension stiffening.

**strain* is defined as the ratio of the difference between the deformed tial length of a fiber to the initial length.

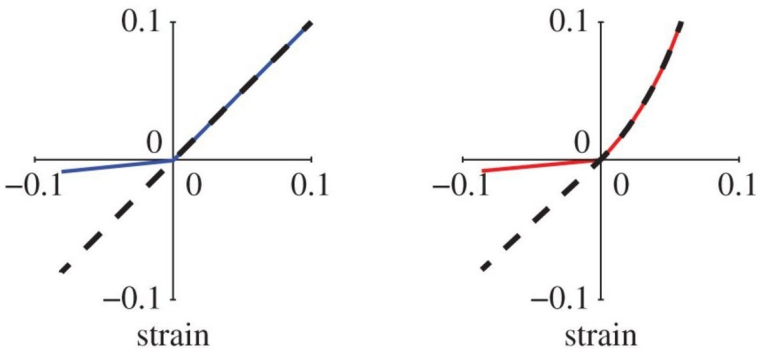

FIGURE 1.5. Notbohn *et al.,* 2015 [23]. Stress-strain curves for **(a)** Dashed black line: linear relation without buckling, i.e. same stiffness in compression as in tension. Solid blue line: **bilinear with buckling**, different slopes in tension and compression. **(b)** Strain-stiffening model. Dashed black line: simulation of non-buckling elements. Solid red line: simulation of buckling elements under compression with a linear relation. Note the abrupt change of stiffness that occurs at the negative values of the buckling (negative) loads.

These finite element simulations provided strong evidence for their formulated hypothesis, that *buckling of fibers enables long-range cell-induced displacements that facilitate mechanosensing*. Particularly, simulations with the bilinear model (Fig. 1.5a, blue solid curve) as well as with the nonlinear model (Fig. 1.5b, red curve) validated the significant contribution of buckling to the slow decay of cell-induced displacements. On the other hand, simulations with the tension-stiffening nonlinear relation but in the absence of fiber buckling in compression (Fig. 1.5b, dashed line) did not result in slow displacement decay, *providing evidence that strain-stiffening alone cannot facilitate the long-range propagation of displacements*.

1.5 Study Overview

The objective of this work is to explore the effects of elastic nonlinearity that fibers exhibit in the Extracellular matrix on deformations induced by embedded contractile cells. For this purpose, we develop a two-dimensional discrete model of a fiber network to simulate deformations induced by cells. The goal is to capture the long-range transmission of displacements due to a contracting cell and, in addition, the formation of inter-cellular bands of dense and aligned fibers, which facilitate the mechanical interaction between cells.

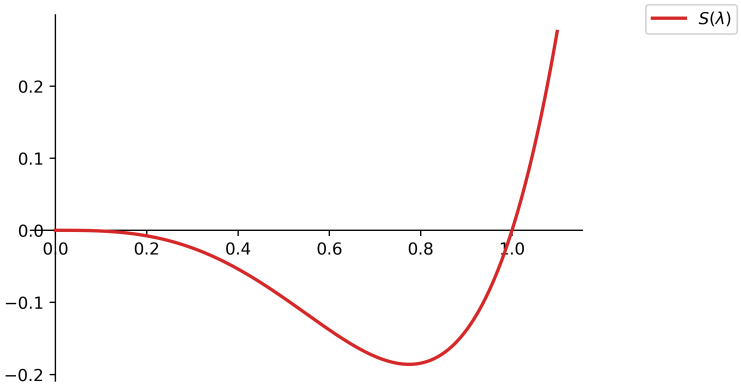

FIGURE 1.6. **Stress - stretch**, $S(\lambda)$, curve of an individual fiber in the proposed model.

Individual fibers are modeled as showing strain stiffening in tension while they lose stiffness under compression owing to buckling. In particular, fibers under tension (for stretches > 1 in Fig. (1.6)), stress is being increased with stretch, so that fibers stiffen as they are being pulled. Fibers under compression, (stretches < 1 in Fig. (1.6)) initially resist to the force that tries to compress them until a critical load is reached which fibers can no longer sustain and thereby buckle. This mechanism deviates from the linear stress-strain* relation in compression-buckling, Fig. (1.5), investigated by the model previously discussed of Notbohm *et al.,* 2015 [23], which was adopted and used with alternations by Sopher and colleagues in [30].

*Stretch, (λ) is defined as the ratio of the deformed length of the fiber to its reference length. The relation with strain e is: e = 1- λ.

CHAPTER 2

METHODS

This chapter contains the methodology we followed in order to build the proposed model. Briefly, the reader can find details regarding both the physical and the computational formulation. Theoretical insights are only provided if necessary, otherwise stated in Appendix.
Before we introduce the geometry of our model (section 2.5) we investigate the mechanical properties that fibers exhibit. In particular, we present the case of a fiber to respond as a common *linear spring* (section 2.4).

Notation:
α ... lower case letters denote a constant scalar
$\mathbf{x}$ ... bold lower case letters denote vectors
$\mathbf{X}$ ... bold upper case letters denote tensors
$\mathbf{I}$ ... identity tensor
x_i ... i component of vector $\mathbf{x}$
X_{ij} ... ij component of tensor/matrix $\mathbf{X}$
IR^n ... n-dimensional Real Vector Space
$\mathbf{G}(\cdot) : IR^n \rightarrow IR^n$ ... vector function of n variables
$G(\cdot) : IR^n \rightarrow IR$ ... scalar function of n variables

The definitions of various concepts are intrduced according to the textbooks [1], [10], [16].

2.1 Formulation of basic concepts

In continuum mechanics materials are modeled as a continuous mass called bodies. Bodies are modeled as regions $\Omega \subseteq IR^3$, where position vectors $\mathbf{x} \in \Omega$ are identified with material points or else particles. Thereby, a body consisting of material points can adopt different states in presence of stimuli, such as forces and heat. These various regions are called *configurations*. In particular, in the absence of applied forces bodies have the so-called natural state. We call this state *reference configuration*. The various configurations that a body can occupy are described using **deformations** from this natural state.

Definition 2.1. Deformation A deformation $\mathbf{f} : \Omega \to \Omega_*$ is a mapping that maps the reference region Ω onto the deformed region Ω_*.

If $\mathbf{x} \in \Omega$ is the reference position of a material point then $\mathbf{y} = \mathbf{f}(\mathbf{x}) \in \Omega_*$ is the position vector of the same particle in the deformed configuration.
Deformations in general cause length and angle changes, at the macroscopic level, which affect the *potential energy* of bonds and the internal forces in a body.
In the following schematic we depict a deformation in a two dimensional vector space, with orthonormal basis $\{\mathbf{e_1}, \mathbf{e_2}\}$:

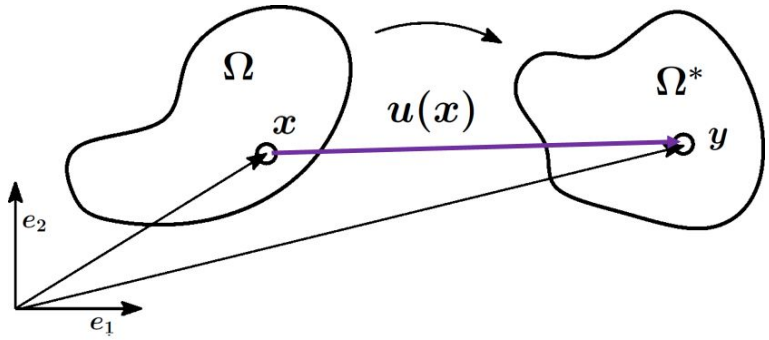

FIGURE 2.1. Deformation in two dimensions. The body occupies the regions $\Omega, \Omega_* \subseteq IR^2$ in reference and deformed configurations respectively. A material point has position vector $\mathbf{x}$ in the reference configuration, while in the deformed configuration its position is given by the position vector $\mathbf{y}$. The mapping $\Omega \to \Omega_*$ is described by the deformation $\mathbf{f} : IR^2 \to IR^2$, $\mathbf{x} \to \mathbf{y}$ or $\mathbf{y} = \mathbf{f}(\mathbf{x})$

.

The vector $\mathbf{u}(\mathbf{x})$ represents the **displacement** of particle $\mathbf{x}$, mathematically defined as the difference between the final and initial position of a particle.

$$\mathbf{u}(\mathbf{x}) = \mathbf{y} - \mathbf{x}$$

(2.1) $$\mathbf{u}(\mathbf{x}) = \mathbf{f}(\mathbf{x}) - \mathbf{x}$$

If we apply the *gradient* with respect to $\mathbf{x}$ to the above equation (2.1),we get that:

$$\nabla \mathbf{f}(\mathbf{x}) = \nabla \mathbf{u}(\mathbf{x}) + \nabla \mathbf{x}$$

$$\mathbf{F} = \nabla \mathbf{u} + \mathbf{I} \tag{2.2}$$

where $\mathbf{F} = \nabla \mathbf{f}(\mathbf{x})$ is the **Deformation Gradient Tensor**, with components:

$$F_{ij} = \frac{\partial f_i}{\partial x_j} \quad i,j = 1,2,3 \tag{2.3}$$

The deformation gradient $\mathbf{F}$ determines local length ratios (deformed/reference length) as well as other geometric changes such as changes in angles or rotations.
Essentially, the deformation Gradient $\mathbf{F} = \nabla \mathbf{f}(\mathbf{x})$ is a matrix, since $\mathbf{f}$ is a vector function. Taking the *determinant* $\det\mathbf{F}$, we have the **Jacobian Determinant**, $\mathscr{J}$, of the mapping $\mathbf{f}$ which defines the local **volume ratio** of the transformed volume devided by the reference volume of a small region around particle with reference position vector $\mathbf{x}$.

Now that we have defined the deformation gradient $\mathbf{F}$ and the geometrical meaning of its determinant, we can refer to the properties of a deformation $\mathbf{f}$:

(i) $\mathbf{f}$ is 1-1, globally invertible, and onto.

(ii) $\mathbf{f} \in C^1(\Omega)$, i.e. is continuously differentiable.

(iii) The Jacobian Determinant $\mathscr{J} = \det\nabla \mathbf{f}(\mathbf{x}) > 0, \forall \mathbf{x} \in \Omega$

Globally invertible in (i) means that different material points cannot occupy the same position in the deformed state:

$$\forall \mathbf{x}, \mathbf{z} \in \Omega : \quad \mathbf{x} \neq \mathbf{z} \Rightarrow \mathbf{f}(\mathbf{x}) \neq \mathbf{f}(\mathbf{z})$$

or equivalenty

$$\mathbf{f}(\mathbf{x}) = \mathbf{f}(\mathbf{z}) \Rightarrow \mathbf{x} = \mathbf{z} \quad \forall \mathbf{x}, \mathbf{z} \in \Omega$$

This property prohibits the ***interpenetration of matter*** (Fig. (2.2)). Interpenetration is the mutual penetration of two objects, one into the other. Objects in physical environment are assumed to be solid and have a defined volume. It makes no sense in the real world to think of one solid object either inside or penetrating another solid object. Accordingly, in the simulation of a physical phenomenon, a model should be intolerant of objects that are interpenetrating.

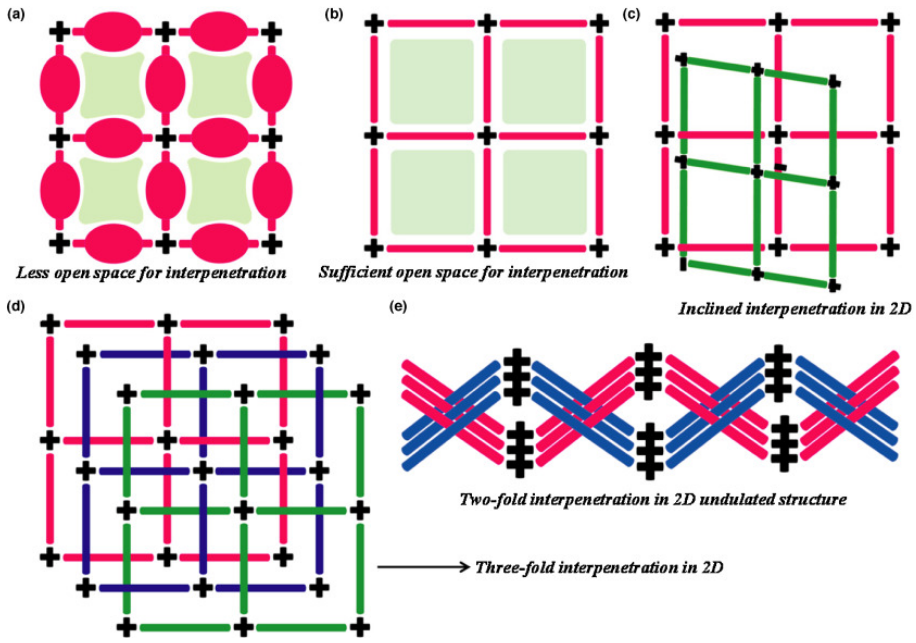

FIGURE 2.2. Representation of two dimensional nets with interpenetration phenomenon: (a) 2D network with no interpenetration, (b) A 2D network with sufficient two dimensional open space, (c, d, e) Different types of interpenetration in 2D networks. *Source: Haldar et al., 2015 [11]*

The positive determinant in (iii) ensures that *orientation* will be preserved in the deformed configuration. Orientation, and thereby the Jacobian determinant, is linked to the interpenetration of a matter, i.e. the inversibility of the mapping describing its deformation by the following theorem:

Theorem 2.1 (Global Inverse Function Theorem)**.** *Let* $\mathbf{f} \in C^1$ *in the interior of* Ω *and suppose that these two conditions are satisfied:*

(i) $det\nabla\mathbf{f} \neq 0$ *in* Ω

(ii) $\mathbf{f}$ *globally* $1-1$ *on the boundary of* Ω

Then $\mathbf{f}$ *globally* $1-1$ *on* Ω.

Zero determinants are not accepted as they refer to matters squeezed down to zero volumes. Note that a negative determinant is also not acceptable. Recall that Jacobian determinant is the ratio of transformed volume to the reference one of a matter. A negative determinant refers to change of its orientation and this change could lead to interpenetration.

2.2 A Discrete mechanical model

Let Ω be a domain, subset of IR^2 with non-empty interior. A discretization of Ω consists of subdomains which are defined as:

Definition 2.2. A subdivision of a domain Ω is a finite collection of element domains K_i. These elements must be located in such a manner, that there are no empty spaces between them and that they do not overlap:

i. $\text{Int}(K_i) \cap \text{Int}(K_j) = \emptyset$, $\forall i \neq j$

ii. $\cup K_i = \Omega$

where $\text{Int}(K_i)$ is the interior, i.e. set of all points in the element K_i, except those which are located on the surface.
If P is the set of all nodes of the discretized domain Ω, then each node $p_k \in P$ has a unique global index $k = 1,\ldots,N$, N is the number of all nodes in the whole discretized domain.

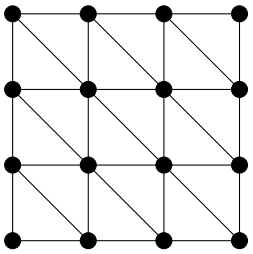

FIGURE 2.3. Triangulation of a square domain

A common discretization is a **triangulation**, in which each element is a triangle:

Definition 2.3. A triangulation of a domain Ω is a subdivision consisting of triangles having the property that no vertex of any triangle lies in the interior of an edge of another triangle.

A discrete mechanical model is represented by a lattice consisting of such elements. Each vertex corresponds to a vector with initial position $\mathbf{p_k} \in IR^2$ for a two-dimensional net, where $k = 1,\ldots,N$, with N to be the total number of vertices. A discrete mechanical model adopts the physical quantities discussed in the previous section as:

- The deformation function $\mathbf{f}$ is a piece-wise affine mapping from initial position $\mathbf{p_k}$ to new position $\mathbf{p'_k}$.
- The displacement $\mathbf{u}$ is the difference between these two positions $\mathbf{p'_k} - \mathbf{p_k}$, for each node k.

For a discrete model, external forces are considered to act **only at the nodes** of the network. The nodes react to these forces by moving accordingly, so that edges connected to them are either being pulled or pressed. Thus, we say that the forces may be either *tensile* or *compressive* to the edges of the lattice.

2.2.1 Orientation

The condition regarding orientation-preservation, i.e., the Jacobian determinant, $\mathcal{J}$, of the deformation gradient $\det\nabla\mathbf{f}$ is required to be positive, page (11), corresponds to a natural physical constraint in elasticity as well as in many other fields.
As previously defined, the Jacobian determinant is the local ratio of deformed volume to the reference one, which in two dimensions is the ratio between the corresponding *areas*. For a triangulized domain, the Jacobian determinant is computed for each element separately. Thus, if we know the initial area covered by each element and its respective deformed area, the Jacobian determinant is known even if the mapping $\mathbf{f}$ is unknown. The area of each element both in reference and deformed configurations can be computed if the initial and final position vectors of their nodes are known.
Consider the following domain consisting of two elements, K_1 and K_2. Assume that a force acting to a node of the network, induces changes that lead to the deformed domain on the right:

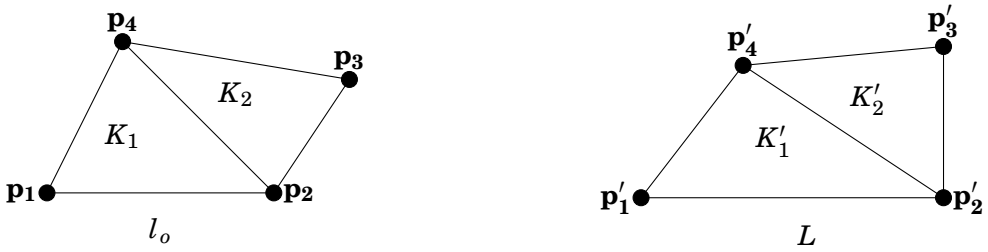

FIGURE 2.4. Reference and Deformed configurations

As depicted in the schematic, each element is defined by nodes $\mathbf{p_k}$, each of which corresponds to a position vector with coordinates (x_k, y_k). Let us work with element K_1, defined by $\mathbf{p_1}, \mathbf{p_2}, \mathbf{p_4}$. The area of K_1 will be given by the **cross product** of the vectors $\mathbf{a}, \mathbf{b}$ as defined below:

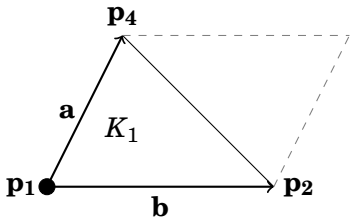

$\mathbf{a} = (a_1, a_2)$ and $\mathbf{b} = (b_1, b_2)$, where a_1, a_2, b_1, b_2 are computed by the coordinates of $\mathbf{p_1}, \mathbf{p_4}$ and $\mathbf{p_1}, \mathbf{p_2}$ as:

$$\mathbf{a} = (a_1, a_2) = (x_4 - x_1, y_4 - y_1)$$

$$\mathbf{b} = (b_1, b_2) = (x_2 - x_1, y_2 - y_1)$$

In mathematics, the cross product is a binary operation on two vectors in three-dimensional space IR^3. Given two linearly independent vectors $\mathbf{a}, \mathbf{b}$, the cross product, $\mathbf{a} \times \mathbf{b}$, is a vector that is perpendicular to both $\mathbf{a}$ and $\mathbf{b}$. The *magnitude* of the resulting vector equals the area of a parallelogram with the vectors for sides, as depicted in the latter schematic.
Since we work in two-dimension space, we introduce the cross product of two vectors in two

dimensions, as a *scalar*:

$$\mathbf{a} \times \mathbf{b} = \epsilon_{ij} a_i b_j \tag{2.4}$$

where $i, j = 1, 2$ and ϵ_{ij} is the *altenator* or *permutation symbol*, in two dimensions, defined as:

$$\epsilon_{ij} = \begin{cases} 0, & \text{if i = j} \\ 1, & \text{if i and j are in cyclic order} \\ -1, & \text{if i and j are in anticyclic order} \end{cases}$$

In particular, we have:

$$\mathbf{a} \times \mathbf{b} = \epsilon_{11} a_1 b_1 + \epsilon_{12} a_1 b_2 + \epsilon_{21} a_2 b_1 + \epsilon_{22} a_2 b_2$$

where, from the definition above, $\epsilon_{11}, \epsilon_{22}$ are zero, while $\epsilon_{12} = 1$ and $\epsilon_{21} = -1$, so we end up with:

$$\mathbf{a} \times \mathbf{b} = a_1 b_2 - a_2 b_1$$

or equivalently,

$$\mathbf{a} \times \mathbf{b} = \begin{vmatrix} a_1 & a_2 \\ b_1 & b_2 \end{vmatrix} = A_{ab} \tag{2.5}$$

where A_{ab} is scalar and denotes the area of the parallelogram that $\mathbf{a}, \mathbf{b}$ form. So, the area of the triangle K_1 will be

$$K_1 = \frac{A_{ab}}{2}$$

Accordingly, we compute the area $A_{a'b'}$ defined by the $\mathbf{a}', \mathbf{b}'$ in order to gain the area of deformed element K_1', using the formula (2.5) for $\mathbf{a}', \mathbf{b}'$.

Thus,

$$K_1' = \frac{A_{a'b'}}{2}$$

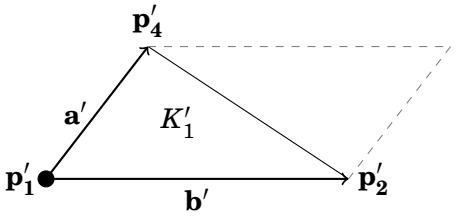

Remark: the vectors $\mathbf{a}, \mathbf{b}$ must be taken with the same direction in both states. For example, one should not compute $\mathbf{a} = \mathbf{p_4} - \mathbf{p_1}$ in initial state and $\mathbf{a}'$ as $\mathbf{p_1'} - \mathbf{p_4'}$ in the final state.

The Jacobian determinant of element K_1 will be:

$$J = \frac{K_1'}{K_1}$$

If the deformed area defined by $\mathbf{a}'$ and $\mathbf{b}'$, gained by their determinant in (2.5), is *negative* this means that the orientation of the specific element has been inverted in the deformed configuration.

Thus, by calculating the two-dimensional cross product, as we defined it, for vectors defining an element, both in reference and deformed configurations, we shall be able to identify where exactly the orientation has been changed, as the Jacobian J will be negative. This part is essential. As we mentioned in previous section, a change in orientation is not physically accepted and thereby, a constraint should be introduced in order to prevent this change. In following chapters, we will discuss further how this constraint has been defined in our model.

2.3 Energy minimization

Physical systems tend to a state of minimum energy. In a discrete model, the particles (nodes) move in order to find a proper arrangement in space so as to reduce the net forces acting on them. Essentially, the lowest energy conformation is the set of lengths and angles between the particles which minimize the forces that would otherwise be pulling nodes together or pushing them apart. In other words, nodes find a compromise among competing forces to determine the lowest energy conformation.
The process of minimizing seeks to find the geometry of a particular arrangement of the particles that represents a *local* or *global energy minimum*.

We have defined a discrete mechanical system as finite collection of *elements* that discretize a reference domain, page (13). In such a discretization, each node corresponds to a position vector. The *coordinates* of each vector are described according to a well defined *Vector Space*. This means that in two dimensions, each node is described by a *pair of two coordinates*. The set of all coordinates in the structure correspond to the *degrees of freedom* of the particular model.

Definition 2.4. The **degrees of freedom** for a given problem are the number of independent problem variables which must be specified to uniquely determine a solution.

Each vertex in a two-dimensional domain has two degrees of freedom.
Let $U(\mathbf{x})$ be the potential energy function where $\mathbf{x}$ is a vector of all vertices' positions. Thereby, if N is the total number of vertices of the domain, the vector $\mathbf{x}$ is a $2 \times N$ dimensional vector and refer to the degrees of freedom set. Each $x_i, i = 1,2,\ldots,N$ is an independent variable for the minimization problem.

2.3.1 Analytical solution

A **global minimizer** of a an objective function f corresponds to a point where the function attains its minimum value. A formal definition is:

Definition 2.5. A point $\mathbf{x}_*$ is a *global* minimum of f, if $f(\mathbf{x}_*) < f(\mathbf{x})$, $\forall \mathbf{x}$

where $\mathbf{x}$ belongs to a range over IR^n or over a domain defined for a particular model.
Accordingly, the **local minimizer** is defined as the point for which the objective function takes the smallest value in its neighborhood:

Definition 2.6. A point $\mathbf{x}_*$ is a *local* minimum of f, if there is a neighborhood $\mathcal{N}$ of $\mathbf{x}_*$ such that

$$f(\mathbf{x}_*) \leq f(\mathbf{x}), \forall \mathbf{x} \in \mathcal{N}$$

where a neighborhood of $\mathbf{x}_*$, $\mathcal{N}(\mathbf{x}_*)$, is defined as an open set that contains $\mathbf{x}_*$.

When the objective function is *smooth* and twice continuously differentiable, local minima are identified using necessary and sufficient conditions for the function's *gradient* and *Hessian matrix*.
Let a function $f : \mathcal{U} \subset \mathbf{R}^n \rightarrow \mathbf{R}$ twice continuously differentiable, $\mathcal{U}$ open and $\mathbf{x}_* \in \mathcal{U}$ a *local optimum*, then $\nabla f(\mathbf{x}_*) = 0$ or:

$$\frac{\partial f}{\partial x_i}(\mathbf{x}_*) = 0 \quad \text{and} \quad i = 1, \ldots, n$$

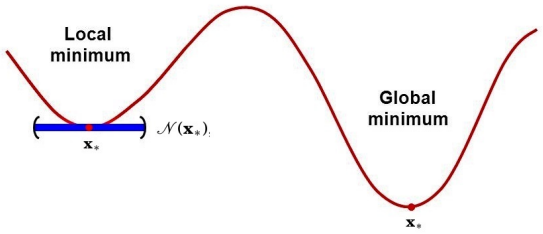

and $\mathbf{x}_*$ is a *critical point* of f. In order to identify whether $\mathbf{x}_*$ is a local maximum or local minimum, we make use of the *Hessian matrix*, the matrix consisting of all the second order partial derivatives of f:

$$\mathcal{H}(\mathbf{x}) = \begin{pmatrix} \frac{\partial^2 f}{\partial x_1 \partial x_1} & \frac{\partial^2 f}{\partial x_1 \partial x_2} & \cdots & \frac{\partial^2 f}{\partial x_1 \partial x_n} \\ \frac{\partial^2 f}{\partial x_2 \partial x_1} & \frac{\partial^2 f}{\partial x_2 \partial x_2} & \cdots & \frac{\partial^2 f}{\partial x_2 \partial x_n} \\ \vdots & \vdots & \ddots & \vdots \\ \frac{\partial^2 f}{\partial x_n \partial x_1} & \frac{\partial^2 f}{\partial x_n \partial x_2} & \cdots & \frac{\partial^2 f}{\partial x_n \partial x_n} \end{pmatrix}$$

at all critical points $\mathbf{x}_*$ under the conditions:

- If $\mathcal{H}(\mathbf{x}_*)$ is *positive definite* then $\mathbf{x}_*$ is a local *minimum*.
- If $\mathcal{H}(\mathbf{x}_*)$ is *negative definite* then $\mathbf{x}_*$ is a local *maximum*.

We know that we can determine the definiteness of a matrix by computing its eigenvalues. Another method is to use the **principal minors**.

Definition 2.7. A *minor* of a matrix A is the **determinant** of some smaller square matrix, cut down from A by removing one or more of its rows and columns.

Definition 2.8. Let M be a symmetric $m \times n$ matrix. A minor of M of order k is *principal* if it is obtained by deleting $n-k$ rows and the corresponding $n-k$ columns of M, where $k = 1,2,\ldots,n$. If the matrix that corresponds to a principal minor is a quadratic upper-left part of the larger matrix, i.e. it consists of matrix elements in rows and columns from 1 to k, then the principal minor is called a *leading principal minor*.

For an $n \times n$ square matrix, such as the Hessian, there are n leading principal minors. We write $\mathscr{D}_k$ for the leading principal minor of order k.

Proposition 2.1. *Let M be an $n \times n$ symmetric matrix. Then:*

- *M is positive definite $\Leftrightarrow \mathscr{D}_k > 0$ for all leading principal minors.*
- *M is negative definite $\Leftrightarrow (-1)^k \mathscr{D}_k > 0$ for all leading principal minors.*

where $k = 1,2,\ldots,n$.

Example 2.1. Let $f(\mathbf{x}) = 2x_1^2 + 3x_1x_2 + 7x_2^2 + 8x_1 + 9x_2 + 10$, where $\mathbf{x} \in IR^2$ the objective function which we want to minimize, which is is twice continuously differentiable. First, we compute the gradient of f with respect to $\mathbf{x}$, as:

$$\nabla f(\mathbf{x}) = (\frac{\partial f}{\partial x_1}, \frac{\partial f}{\partial x_2}) \quad or \quad \nabla f(\mathbf{x}) = (4x_1 + 3x_2 + 8, \quad 3x_1 + 14x_2 + 9)$$

Then, we have search for *critical points*, for which the gradient is zero:

$$\begin{cases} 4x_1 + 3x_2 + 8 = 0 \\ 3x_1 + 14x_2 + 9 = 0 \end{cases}$$

This system has solution for:

$$\mathbf{x}_* = \begin{cases} x_1 \approx -1.80851 \\ x_2 \approx -0.25532 \end{cases}$$

So this $\mathbf{x}_*$ is the only critical point. We continue by computing the second order derivatives of f on this point, in order to construct the Hessian matrix:

$$\frac{\partial^2 f}{\partial x_1^2} = 4, \quad \frac{\partial^2 f}{\partial x_2^2} = 14, \quad \frac{\partial^2 f}{\partial x_1 \partial x_2} = \frac{\partial^2 f}{\partial x_2 \partial x_1} = 3$$

so, the Hessian matrix at critical $\mathbf{x}_*$ is:

$$\mathscr{H}(\mathbf{x}_*) = \begin{pmatrix} 4 & 3 \\ 3 & 14 \end{pmatrix}$$

for which the **leading principal minors** are:

$$\mathscr{D}_1 = 4 > 0, \qquad \mathscr{D}_2 = \begin{vmatrix} 4 & 3 \\ 3 & 14 \end{vmatrix} = (4 \cdot 14) - 9 = 47 > 0$$

Both $\mathscr{D}_1, \mathscr{D}_2$ are positive, thereby according to proposition (2.1) the Hessian matrix of function f is **positive definite** at the critical point $\mathbf{x}_*$, thus $\mathbf{x}_*$ is a **local minimum** for function f.

2.3.2 Numerical optimization

In *unconstrained optimization*, the objective function depends on real variables and is being minimized with no restrictions regarding the values these variables can take.

$$\min_{\mathbf{x}} f(\mathbf{x})$$

where $\mathbf{x} \in IR^n$ a vector with $n > 1$ components and $f : IR^n \rightarrow IR$.
There is a number of optimization algorithms that are being widely used for unconstrained minimization. These algorithms are basically iterative procedures that terminate when either no more progress can be made or when it seems that a solution point has been approximated with sufficient accuracy.
Briefly, each algorithm starts with an initial guess $\mathbf{x_0}$. At each iteration k, the algorithm evaluates the objective function at current $\mathbf{x_k}$, while it may take take into account previous iterates as well, $\mathbf{x_0}, \mathbf{x_1}, \ldots, \mathbf{x_{k-1}}$, in order to decide whether they should terminate or find a new iterate $\mathbf{x_{k+1}}$ with a lower function value than $\mathbf{x_k}$.
There are two basic iterative approaches for moving from the current point $\mathbf{x_k}$ to a new $\mathbf{x_{k+1}}$, the *line search* and the *trust region*. The line search approach first finds a **descent direction** along which the objective function will be reduced and then computes a step size that determines how far $\mathbf{x}$ should move along that direction. There is a number of methods that compute the descent direction. In this study, we have chosen the *Quasi-Newton* method and the *Nonlinear conjugate gradient* method for the minimization problem defined in the next section.

2.3.3 Elastic Potential Energy

Elastic energy is the potential mechanical energy stored in the configuration of a material as work is performed to distort its volume or shape. Elastic energy occurs when objects are deformed in any manner, for example they are either being compressed or stretched. The essence of elasticity is *reversibility*. Forces applied to an elastic material transfer energy into the material which upon yielding that energy to its surroundings can recover its original shape.

Potential energy (U) is the stored energy of a system which is depended only upon the relative position of its various particles. The Potential energy arises in systems with particles that exert forces on each other. It is equal to the negative of the work done by these forces which depends only on the initial and final positions of the particles. These forces, are called *conservative forces*.

If the exerted force is known, and is a conservative force, then the potential energy can be obtained by:

$$U = -\int_{\mathbf{x_i}}^{\mathbf{x_f}} \mathbf{F} d\mathbf{x} \tag{2.6}$$

where $\mathbf{x_i}$,$\mathbf{x_f}$ are the reference and final position vectors of the system, respectively. In the Fig. (2.5), $\mathbf{x_i}$ corresponds to the position A of the particle on which a force is applied and $\mathbf{x_f}$ corresponds to the final position B the particle obtains under the work of the applied force.
For the exerted force we have:

$$\mathbf{F} = -\nabla U \tag{2.7}$$

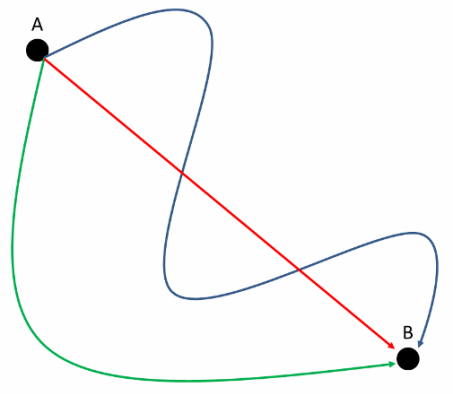

FIGURE 2.5. Three potential paths for a particle to move from point A to point B. All of them require the same amount of work, if the exerted force is conservative. Thus, the potential energy depends only on the points A, B and not on the path that the point followed.

For a discrete model, the total potential energy is a *summation* over elements energy values. The energy of each element corresponds to a summation over the individual energy values of the edges defining it and depends only on the reference and final position vectors of the nodes. Thus, **the total potential energy of a discrete model is a summation over all edges' stored energy values**.
Consider the following square network consisting of two elements T_1, T_2:

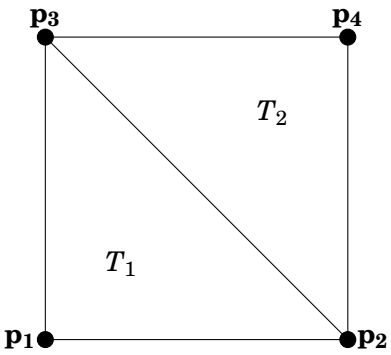

Each node in the network corresponds to a position vector $\mathbf{p_n}, n = 1,2,3,4$, with two coordinates (x_n, y_n), so that each nodes has two degrees freedom (2.4, on page 16).
Let PE be the total potential energy of this system. According to what stated above for the system's energy, we have:

$$PE = U_1 + U_2 + U_3 + U_4 + U_5$$

where U_k, refers to the potential energy stored in edge k

We define each one of U_k, k the total number of edges of a network, as a scalar function that is twice continuously differentiable and depends only on the position vectors of the nodes that edge k connects.

Definition 2.9. Let a two dimensional discrete model defined by n nodes and k edges. The energy stored in **each edge** is given by a twice continuously differentiable function $\Phi : IR^4 \rightarrow IR$:

$$U_k = \Phi(\mathbf{p_k}) \tag{2.8}$$

where $\mathbf{p_k}$ is the vector containing each pair of coordinates of each node of the edge k. Essentially, $\mathbf{p_k}$ is a vector with the degrees of freedom of these nodes, and since each node has two degrees of freedom, for a two dimensional model, the dimension of $\mathbf{p_k}$ will be four.

Thus, the total potential energy of the network in question will be given by:

$$PE = \sum_{i=1}^{k} U_k \tag{2.9}$$

which is twice continuously differentiable as a sum of continuously differentiable functions. The total potential energy PE will be a function depending on all nodes in the network, and by that, on the total number of degrees of freedom. So, for a network with total n nodes, the degrees of freedom will be $2 \times n$.
For now on, we will refer to the degrees of freedom vector for a given network as $\mathbf{x}$.

The minimization problem for a two dimensional network with n nodes is formulated as:

$$\min_{\mathbf{x}} PE(\mathbf{x}) \tag{2.10}$$

where $\mathbf{x}$ a vector with $2 \times n$ components and $PE : IR^{2\times n} \rightarrow IR$, the objective energy function to be optimized, under the **Minimum Potential Energy Principle** which states that:

For conservative structural systems, of all the kinematically admissible deformations, those corresponding to the equilibrium state extremize (i.e. minimize or maximize) the total potential energy. If the extremum is a minimum, the equilibrium state is stable.

2.4 The Linear Springs case

The **linear spring** is a common example of an elastic material, whose elastic potential energy is the result of a work done to either stretch or compress it. According to ***Hooke's law***, the force required to extend or compress the spring by a distance x is linearly proportional to this distance:

$$\mathbf{F} = k\mathbf{x}$$

However, Hooke's law is often used under the convention that this force is the *restoring load* exerted by the spring as it is being deformed due to an external load, so that: the restoring force **F** is negative as it has the opposite direction of that the spring's end tends to move due to the external load. The parameter k in these formulas is a constant which exploits the *stiffness* of a spring.

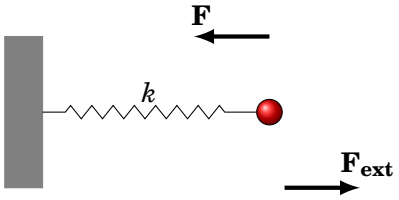

(2.11) $$\mathbf{F} = -k\mathbf{x}$$

From equations (2.6), (2.11), the **potential energy of a spring** is given by:

$$U = -\int_{x_0}^{x} -k\mathbf{x}d\mathbf{x}$$

or:

(2.12) $$U = \frac{1}{2}k\mathbf{x}^2 + U(\mathbf{x_0})$$

where $U(\mathbf{x_0})$ is the potential energy for the undeformed spring, arbitrarily taken as zero.
In the schematic (2.6), we see that the external load on the red mass has stretched the one-dimensional spring to deformed length L. Let $F_{ext} = 10$ newton and the stiffness constant $k = 1.0$. In order to find the *static equilibrium* of the system we make use the **force - balance principle**. According to this principle the sum of all forces applied to the system should be equal to zero. There are two forces to be considered here: $F_{spring} = -kx$ and F_{ext}, for which the force-balance principle is:

$$F_{spring} + F_{ext} = 0$$

that results in:

$$-kx = -F_{ext}$$

or

$$x = \frac{F_{ext}}{k}$$

And for the given values of k, F_{ext}, the equilibrium for this system is at

$$x_{eq} = 10$$

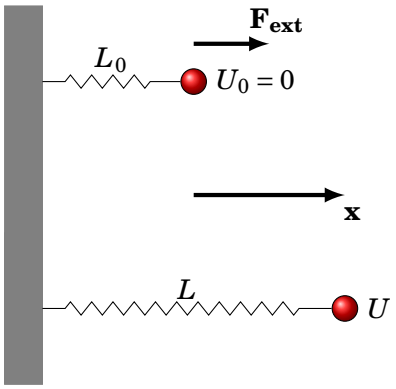

FIGURE 2.6. Stretch of a spring due to external load $\mathbf{F_{ext}}$

.

We can reach the same result by using the **Minimum Potential Energy** principle, as previously defined on page (21), instead of the force-balance method. The Potential Energy, PE of this system is the sum of the energy stored in the spring,U, plus the work potential. The work potential is the *negative* of the work done by the external force acting on the system.
Work done by the external forces is simply the forces multiplied by the displacements at the points of application of forces. So, here we have:

$$PE(x) = U + (-F_{ext}x)$$

$$PE(x) = \frac{1}{2}kx^2 + (-F_{ext}x)$$

The value of x that extremizes this function corresponds to the equilibrium state.
In order to find the extrema of a function, we have to evaluate the critical points. Thus, we have:

$$\frac{d}{dx}(\frac{1}{2}kx^2 - F_{ext}x) = 0$$

which results in the critical point

$$x_{eq} = 10$$

At this point, the potential energy is

$$PE(10) = -75J$$

and in order to see if this point refers to a minimum or maximum, we check the sign of the second derivative of PE at x_{eq}:

$$\frac{d^2}{dx^2}(\frac{1}{2}kx^2 - F_{ext}x) = k > 0$$

which means that at $x_{eq} = 10$ the potential energy takes its *minimum* value $-75\ J$.

Remark: We can write the displacement **x** of the node at the end of the spring as the difference between the deformed and the reference lengths:

$$U = \frac{1}{2}k(L - L_0)^2 \tag{2.13}$$

which gives the total elastic potential energy placed into a single spring, that is being stretched, or compressed, from initial length L_0 to final length L.

Following, we move on two two dimensions and investigate how a system of three springs respond to external stimulus. The springs are connected to form a triangle, since the discretization of the proposed model will be in triangles and we want to investigate the possible states that an element can reach, under the application of various initial conditions. The points at which the springs are connected are the nodes in each system, on which we apply these conditions; either we let them free to move or keep them fixed at their origin. Depending on each case's conditions, we form the potential energy of the system and minimize it, in order to find the local minimum, if any, for which the system is stabilized.

Case I: One node free

Consider the system of three linear springs, like those in Fig.(2.4), connected at the vertices with position vectors $\mathbf{p_n}$, $n = 1,2,3$ and coordinates (x_i, y_i), $i = 1,2,3$, i.e. (x_1, y_1), (x_2, y_2), (x_3, y_3) for $\mathbf{p_1}$, $\mathbf{p_2}$, $\mathbf{p_3}$ respectively. In this case, two nodes are kept fixed, while the third is free to move, after a load exerted on it. First, we consider different rest length, L_n, for each spring and different stiffness constants k_n as well.

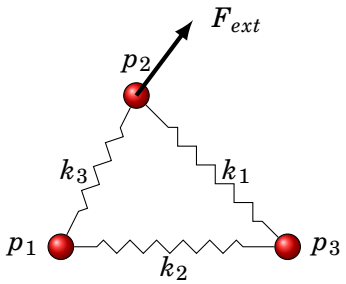

FIGURE 2.7. Two nodes fixed at their origin and one, $\mathbf{p_2}$, free to move.

The reference position vectors for the three nodes are:

$$\mathbf{p_1} = (0,0), \quad \mathbf{p_2} = (1,2), \quad \mathbf{p_3} = (3,0)$$

Therefore, the rest length L_n of each spring k_n is:

$$L_1 = 2\sqrt{3}, \quad L_2 = 3.0, \quad L_3 = \sqrt{5}$$

respectively, with stiffness constants $k_1 = 1.5$, $k_2 = 1.0$ and $k_3 = 1.0$. We apply a force $\mathbf{F_{ext}} = (F_x, F_y) = (6,8)$ at vertex $\mathbf{p_2}$, as shown above, while keeping the other two vertices fixed. The aim here is to find the equilibrium state, which corresponds to evaluating the coordinates (x_2', y_1') of vector $\mathbf{p_2'}$, which is the deformed position vector of node with reference position vector $\mathbf{p_2}$

Let L_n' be the deformed length of spring n. Since the load is exerted only on $\mathbf{p_2}$, the springs connected to it, k_1, k_3 will be deformed but k_2 will not. The deformed lengths of these two springs are given by:

$$L_1' = |\mathbf{p_2'} - \mathbf{p_3}|$$

$$L_3' = |\mathbf{p_2'} - \mathbf{p_1}|$$

where $\mathbf{p_1} = (x_1, y_1) = (0,0)$, $\mathbf{p_3} = (x_3, y_3) = (3,0)$. The two deformed lengths are calculated as:

$$L_1' = \sqrt{(x_2' - x_3)^2 + (y_2' - y_3)^2} \tag{2.14}$$

$$L_3' = \sqrt{(x_2' - x_1)^2 + (y_2' - y_2)^2} \tag{2.15}$$

Making use of the formula (2.13), the **potential energy** of the system will be given by the sum of the energy U_n stored in each deformed spring, in terms of their respective lengths, plus the work potential:

$$PE = \frac{1}{2}k_1(L_1' - L_1)^2 + \frac{1}{2}k_3(L_3' - L_3)^2 - \mathbf{F_{ext}} \cdot \mathbf{p_2'} \tag{2.16}$$

where L_1', L_3' are given by (2.14), (2.15). The

In order to find the equilibrium state, we evaluate the position vector of node p_2 in the deformed state, by minimizing the potential energy. First, we have to compute the two partial derivatives of PE with respect to the unknown coordinates x_2, y_2 of the vector $\mathbf{p_2'}$

The partial derivative of (2.16) with respect to x_2' is:

$$\frac{\partial PE}{\partial x_2'} = k_1(\sqrt{(x_2' - x_3)^2 + (y_2' - y_3)^2} - L_1)\frac{1}{\sqrt{(x_2' - x_3)^2 + (y_2' - y_3)^2}}(x_2' - x_3) + k_3(\sqrt{(x_2' - x_1)^2 + (y_2' - y_1)^2} - L_3)\frac{1}{\sqrt{(x_2' - x_1)^2 + (y_2' - y_1)^2}}(x_2' - x_1) + F_x$$

and with respect to y_2':

$$\frac{\partial PE}{\partial y_2'} = k_1(\sqrt{(x_2' - x_3)^2 + (y_2' - y_3)^2} - L_1)\frac{1}{\sqrt{(x_2' - x_3)^2 + (y_2' - y_3)^2}}(y_2' - y_3) + k_3(\sqrt{(x_2' - x_1)^2 + (y_2' - y_1)^2} - L_3)\frac{1}{\sqrt{(x_2' - x_1)^2 + (y_2' - y_1)^2}}(y_2' - y_1) + F_y$$

and both of them must satisfy

$$\frac{\partial PE}{\partial x_2'} = \frac{\partial PE}{\partial y_2'} = 0$$

All pairs x_2', y_2' for which the latter condition holds, are the critical points of PE.

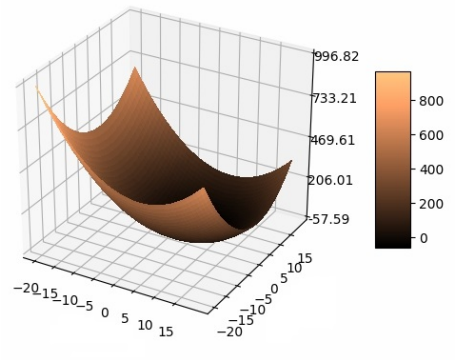

We evaluate the potential energy in the grid (-20,20) and we see that it exploits the behaviour of a *convex* function. This is an indication that there should be one (global) minimum.

Indeed, the algorithm results in a specific minimum, Fig. (2.8 a), and the deformed configuration at which the system is in equilibrium is depicted in Fig. (2.8 b) against the reference one.

We were also interested to see what the equilibrium states would be if *no loads* at all were applied on the free node (p_2). In Fig. (2.8 a) and (2.8 b) it is clear that in a system of one free to move node, in the absence of external forces, the system will sustain the rest length of each spring.
Since one node is free to move, in order to preserve the lengths of the two springs that are connected to it, it can only move to its symmetrical node with respect to the x axis. Although, moving to this symmetrical point results in changing the system's *orientation*.

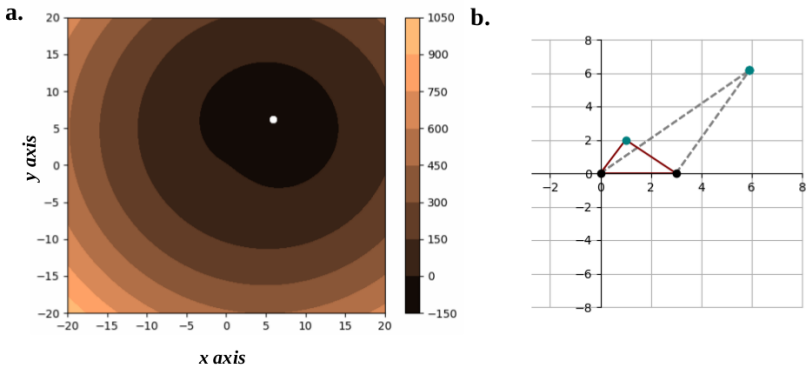

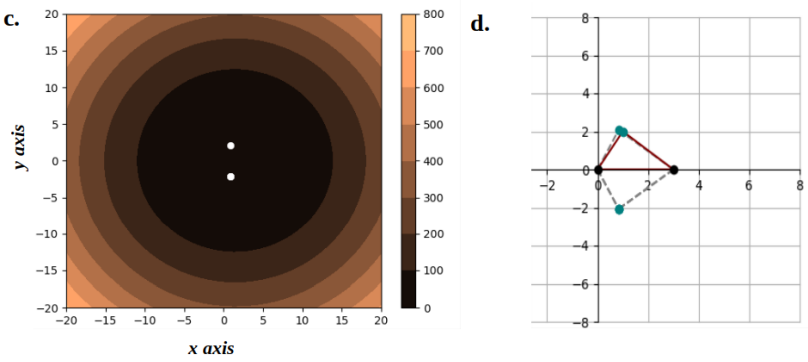

FIGURE 2.8. Equilibrium states for a triangular spring system. **(a)** Contour plot of the system's potential energy. The white dot corresponds to the *minimum* point for which the system is at equilibrium. **(b)** Reference (dark red) and deformed (gray dashed) configurations for the system, the blue node corresponds to the free one. **(c)** Contour plot of the energy and two points as minima, in the absence of forces. These two points are symmetrical to *x axis*. **(d)** When no loads are exerted on the system, it will sustain the reference lengths of the springs, while the free node has two preferable positions which are symmetrical. Their difference lies in the *orientation* of the system. Clearly, for the *dashed* triangle the orientation has been inversed.

Following, we want to investigate whether and how the *fixed parameters* of the system influence its deformation. Fixed parameters include the constants k and the springs' rest lengths. Thus, we consider now three springs forming an equilateral triangle, Fig. (2.9 a) and have the same stiffness constant k. The node with reference position vector $\mathbf{p_2}$ is free to move, as before, and we evaluate here the potential energy behaviour, as well as the system's state in the absence of forces.

The behaviour of function (2.16) is extremely different from the one we saw in the previous case, Fig. (2.9 b). We detect here multiple *critical points*. In particular, we have two local *maxima*, two *minima* and and one *saddle point*.

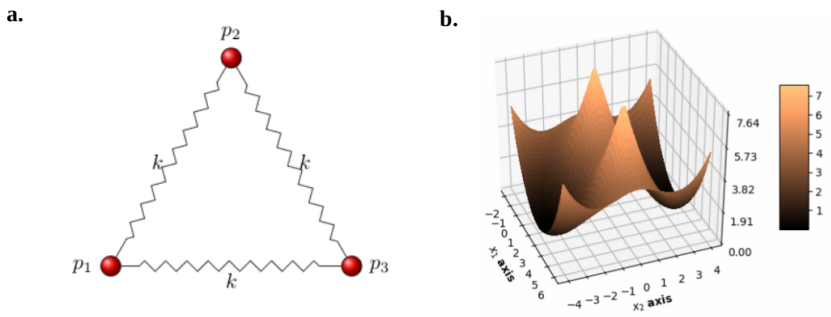

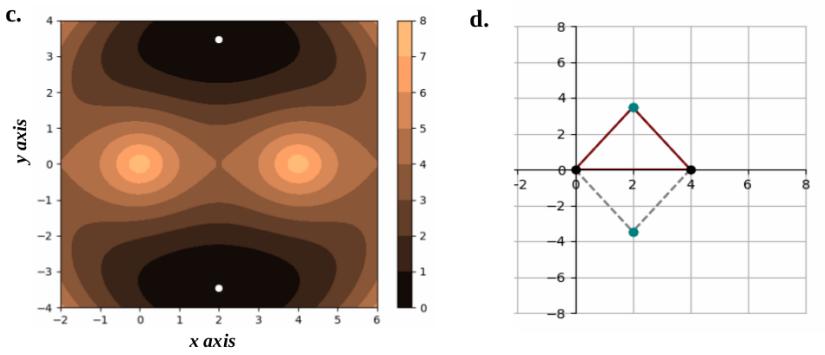

FIGURE 2.9. Behaviour of an equilateral spring system with same stiffness constant k for each spring, when one node is not fixed and there is no external stimulus on any node. **(a)** A schematic of the system, the node with position vector $\mathbf{p_2}$ is free to move. **(b)** The potential energy behaviour of the system. Clearly, there are multiple critical points. **(c)** Contour plot of the system's potential energy. The white dots correspond to the *minima* points, for which the system is at equilibrium, and are the precise positions that the free node may take in order to sustain the system's configuration. **(d)** The two configurations for the system, the blue node corresponding to the free one. When no loads are exerted on the system, this will sustain the reference lengths of the springs, while the free node has two preferable positions which are symmetrical. Their difference lies in the *orientation* of the system. Clearly, for the *dashed* triangle the orientation has been inversed.

In the respective contour plot, Fig. (2.9 c) we see the two local *minima* being symmetrical to the x *axis*, as before. These two minima, as it was expected, correspond to the same configuration for the equilibrium state, i.e. two symmetric to x *axis* position vectors for the free node, Fig. (2.9 d). Clearly, the choice of parameters is of significant importance.

Finally, we discriminate the following cases; first, we consider a triangle system with one fixed node while forces are applied on the other two and, second, we assume a system for which there is a load exerted on each node. In the latter case, since all nodes are free to move, the forces have been chosen so that the *net* force is zero, in order for the system to satisfy the *force-balance* law, Fig. (2.10).
In addition, we constructed systems with more *springs* connected together in triangularized rectangular structures, Fig. (2.11). In particular, each rectangle is divided into smaller ones which are further divided into triangles, producing four possible structures. For each one of these structures, we keep *fixed* the nodes of the lower boundary. In this case, instead of applying a force on some nodes, we impose **Dirichler boundary conditions** on the upper boundary. Especially, we set every node of the upper boundary a displacement $\mathbf{u} = (h, 0.0)$, where h is the scale to which each one of boundary nodes will move along the x direction. We then minimize the system's energy accordingly. Results for these cases in the respective figure-caption.

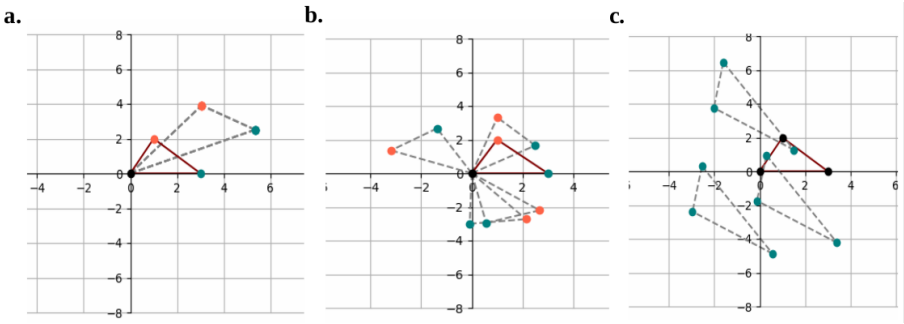

FIGURE 2.10. Forces on two or three nodes for triangular spring system. **(a)** two forces act separately on two different nodes while the third is kept fixed at its origin (black node). Reference (dark red) and deformed (dashed) configurations of the system, after the two-loads application. **(b)** The same system (dark red - reference state) in the absence of loads stays in its original state, letting the two free nodes to move so that each spring is not either *stretched* or *compressed*; the lengths are being preserved. In other words, since the two nodes are free to move in any direction by keeping the lengths at their initial length, we expect to see infinite **reflections** of the reference state-triangle with respect to the fixed at $(0,0)$ node. **(c)** Each node is free to move and we have three forces, each one act on a different node. The net force for the system should be zero, i.e. $\mathbf{F} = \mathbf{F_1} + \mathbf{F_2} + \mathbf{F_3} = \vec{0}$. Each *dashed* triangle refers to the deformed configuration and is the result of each independent run of the algorithm. Since all nodes can move to any direction, there are *infinite* solutions for the system's equilbrium state.
Notice: Each of these triangles will always be the same (lengths and angles preserved in each dashed triangle). The position vectors may change coordinates but the whole area and shape of the triangles they form will not. Thus, the system's multiple equilibria are **translations** of the same triangle.

The special case of *Linear springs* gave us an intuition of what we should expect regarding the behaviour of our model and, in particular, in what way the model's edges would respond to some form of traction and what changes this response may induce to its geometry and its orientation as well. Especially, we note the important issue of interpenetration, more clearly depicted in final case, Fig. (2.11). Even if mathematically the system reaches its equilibrium with this particular rearrangement of its particles, physically the mutual penetration of the system's triangles one into the other cannot be accepted.

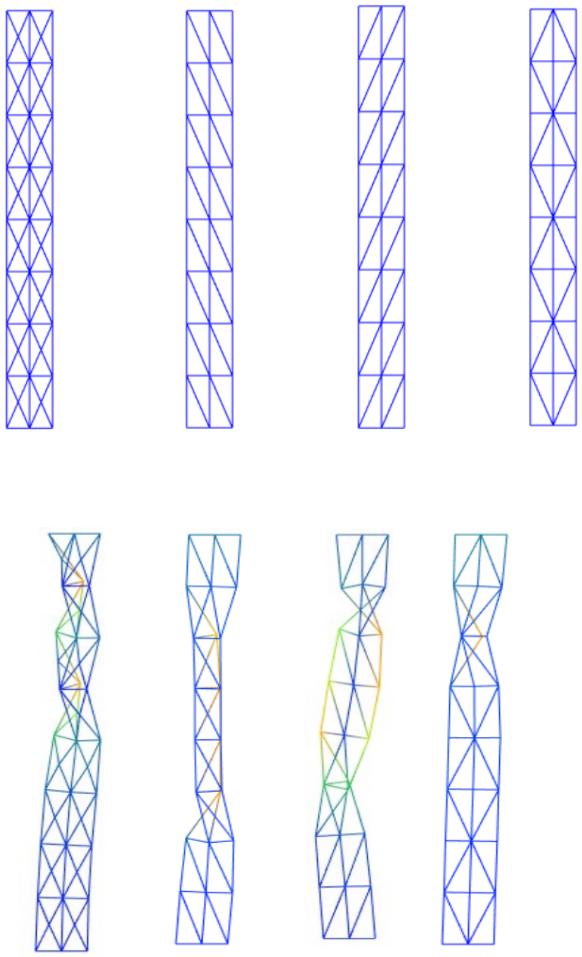

FIGURE 2.11. Rectangular systems. **(a)** Each rectangle is divided into smaller ones, and each one of the small rectangles is divided into two triangles, resulting in four different structures: (i) *crossed* diagonals in each small rectangular, (ii) only *left* diagonal, (iii) only *right* diagonal and (iv) *right-left* diagonal in turn. The lower boundary (base) is kept fixed, i.e. each nodes cannot move. We apply Dirichlet boundary conditions on the upper boundary. In particular, we impose a displacement $\mathbf{u} = (h, 0.0)$, h being the scale to x direction, on each one of the nodes of the upper boundary. The total energy of the system will be a sum of the individual edges' energy. **(b)** The resulting equilibrium state for each one of the four systems. Each state corresponds to **interpenetration**. We note that the *right-left* structure seems to be more stable in this case, but the problem still remains.

2.5 The Model

We develop two-dimensional triangularized networks of straight edges representing the fibers and investigate two phenomena:

i. the localized displacements induced in the fibrin matrix by one embedded contracting cell.

ii. the physical mechanism of tether formation between two contracting cells.

2.5.1 Network geometry

The two dimensional network represents the Extracellular matrix (ECM) and is modelled as a disk of radius A, centered at the origin $(0,0)$.

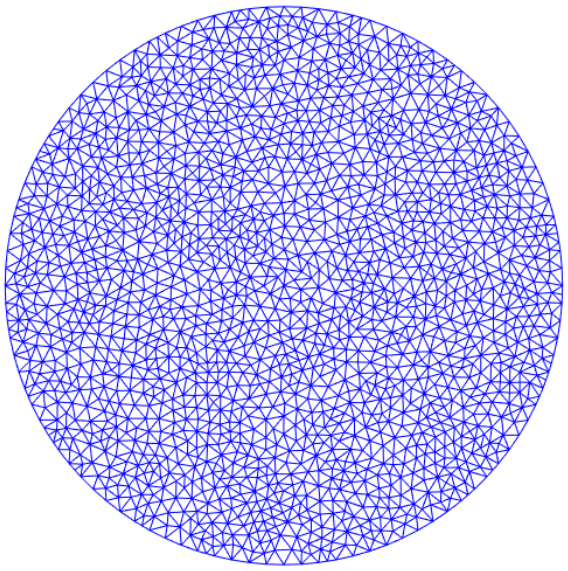

FIGURE 2.12. A typical triangularized domain of our model with radius $A = 10$ units and resolution 30.

Such a conformation, Fig. (2.12), is called *mesh* and constitutes the *domain* of our model. The geometry of the domain plays a significant role in the way that the matrix is deformed. In particular, the number of nodes indicates the number of degrees of freedom, i.e. the independent variables of the minimization problem. A domain with a larger number of connected nodes serves more options for them to move and thereby induce larger deformations in the matrix. In addition, the number of nodes is linked to the total number of elements (triangles) and to their size as well. This means that, a mesh with less vertices would consist of triangles with much bigger areas compared with a more dense one where the triangles' faces are much smaller. The parameter that induces a refinement of a mesh, by either increasing or decreasing the number of nodes, is called *resolution*. The bigger this number is, the more dense a mesh is. For example, in Fig, (2.12) the generated mesh has resolution 30.
There are some additional aspects that characterize a mesh'es geometry and its refinement:

(a) *hmax*: The maximum element diameter over all elements, which corresponds to the largest edge of the mesh.

(b) *hmin*: The minimun element diameter. Accordingly to hmax, hmin corresponds to the shortest edge of the mesh.

(c) C: The connectivity of the network which is the average number of edges meeting at a node.

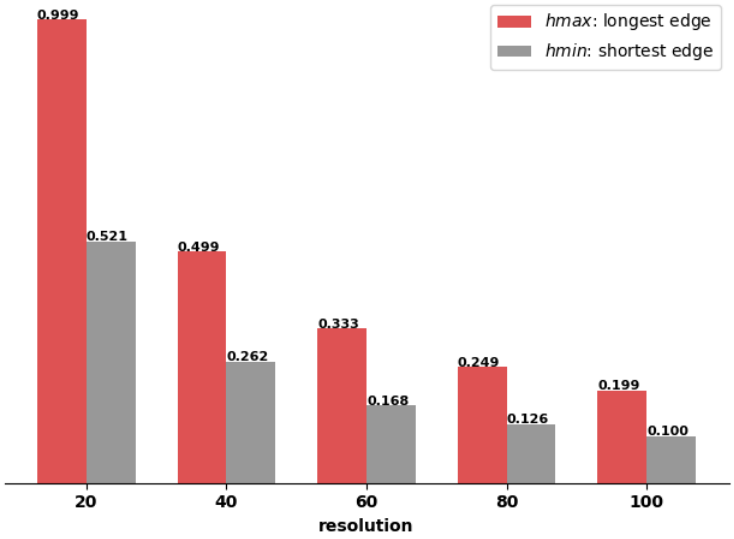

Starting with a mesh of *resolution* 20 and gradually double, triple it and so on, reaching a resolution 100 we see that the longest and shortest length of each refined mesh **decrease proportionally**. (radius of mesh $A = 10$)

In general, the network is refined by adding midpoints between two nodes along each edge. The longest edge in initial mesh with resolution 20 had length $l_o = 0.999$. By doubling the resolution to 40, an extra node has been added in the middle of each edge. Thereby, the length l_o has been divided in half so that in the new mesh with resolution 40, the longest edge has 0.499, half of l_o. By tripling the resolution to 60, edges' lengths are divided by three and so on.

In a disk like the one in Fig. (2.12) with radius A, **an embedded cell** is modelled as a smaller disk of radius α, centered in the origin $(0,0)$. Thus, we gain an *annulus*, that represents the Extracellular matrix (Fig. 2.13). For this structure, we have $\alpha < r < A$, where r is the *radial distance* of a position vector $\mathbf{x}$ from the cell centre $(0,0)$, so that:

$$r = |\mathbf{x}|$$

In particular, we model a cell's **contraction**, meaning that the cell shrinks. To address this, we apply a *radial displacement* $u(r)$, a scalar, on the cell's boundary.
The displacements with radial symmetry are given by:

$$\mathbf{u}(\mathbf{x}) = u(r)\frac{\mathbf{x}}{r} \tag{2.17}$$

for a node with position vector $\mathbf{x}$. On cell's boundary each node has $r = \alpha$ and undergoes an *inward* radial displacement

$$u(\alpha) = -u_0, \quad u_0 > 0 \tag{2.18}$$

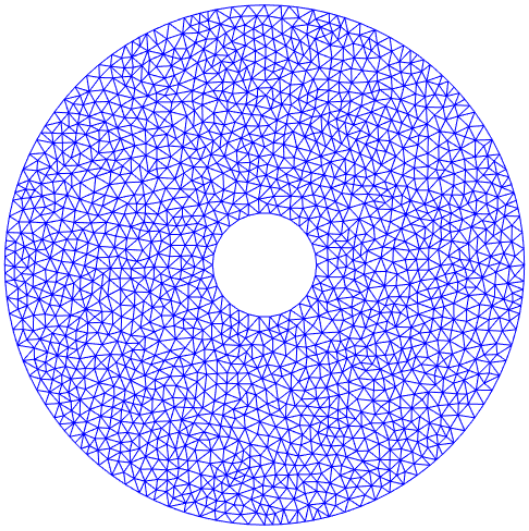

FIGURE 2.13. The network representing the contracting cell model. For the two radii we have $A = 10$ and $\alpha = 2$. The cell undergoes contractile, i.e. inward, radial displacement $u(\alpha)$ (not shown here).

For the **two-cells model**, we work in the same way. Two circular regions representing cells embedded within the ECM (large disk). The centers of both circles are coincident with the horizontal line passing through the origin (0,0) of the network. On each one's boundary, a radial displacement is imposed to simulate their contraction.

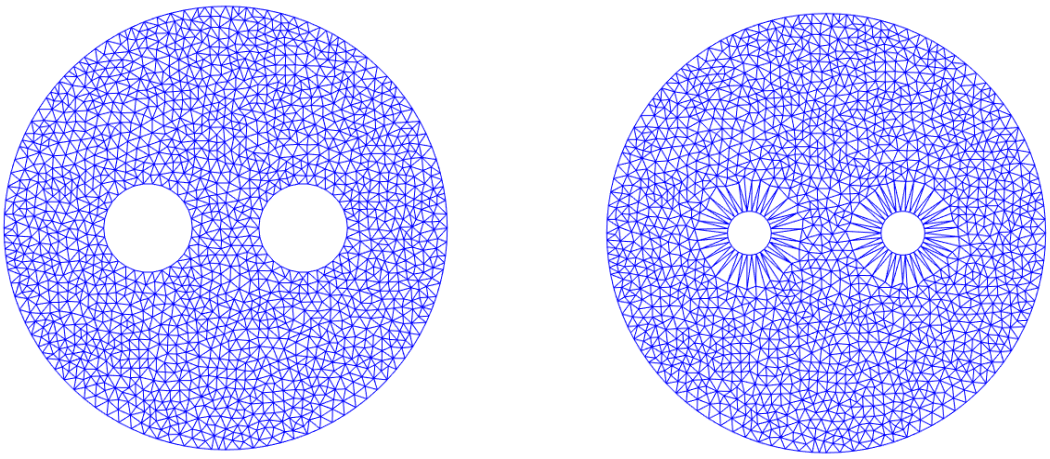

FIGURE 2.14. ***Left*:** Two cells model. The disk of radius 10 include two cells of radius $\alpha = 2$ and distance 7 between their centers. ***Right*:** A radial displacement of $u(\alpha) = -1.0$ applied on both of them results in contraction to half of their initial radius.

We discriminate two cases, for both of these models, regarding the outside boundary of the large disk. The outside boundary may be either:

i. *traction free*: the nodes on the boundary are free to move.

ii. *fixed*: zero displacement as condition for all nodes on its boundary, i.e. they are fixed at their initial positions.

2.5.2 Mechanical properties

In each one of our networks, we include circles representing the cells, as we discussed in previous section (Fig. (2.14)). Under cell contraction, deformations are induced in the networks due to the displacements of the network's nodes. Each pair of nodes is connected by an edge which represents an individual fiber. As nodes rearrange, they apply forces to the fibers resulting in either their tension ($L > l_o$) or compression ($L < l_o$), where l_o is the reference length of a fiber and L denotes its deformed length.
To begin with, we introduce the **stretch ratio**, λ, of each fiber, defined as the deformed fiber length divided by the reference fiber length:

$$\lambda = \frac{L}{l_o} \tag{2.19}$$

where L is the deformed and l_o the reference length of the fiber. We have the following relations:

$$\lambda : \begin{cases} > 1, & L > l_o \\ = 1, & L = l_o \\ < 1, & L < l_o \end{cases} \tag{2.20}$$

The proposed mechanism which facilitates the phenomena we wish to examine is **buckling of fibers under compression**. The simulation of buckling is described by the non-linear relation between force ($\mathscr{S}$) and stretch (λ) in each fiber, given by:

$$\mathscr{S}(\lambda) = k(\lambda^5 - \lambda^3) \tag{2.21}$$

The force $\mathscr{S}$ is defined as the derivative of the energy of a fiber with respect to stretch λ, recall (2.7) on page (20). Thus, taking the integral of equation (2.21) above, we gain the energy formula of an individual fiber, denoted with $\mathscr{W}(\lambda)$:

$$\mathscr{W}(\lambda) = k\left(\frac{\lambda^6}{6} - \frac{\lambda^4}{4} - \frac{1}{6} + \frac{1}{4}\right) \tag{2.22}$$

In these equations, k is the **stiffness constant** of each fiber.
The behaviour of these two functions is depicted below:

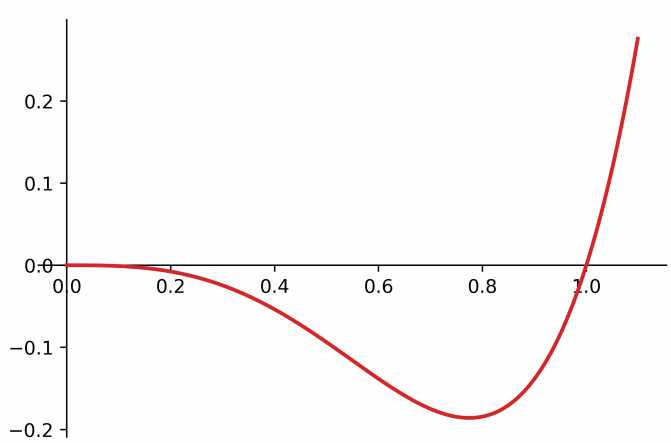

FIGURE 2.15. $\mathscr{S}(\lambda)$

(a) Upon *tension*, $\lambda > 1$, the fiber exhibits a non-linear behaviour. Force and stiffness (slope of the curve) increase with λ in tension. This refers to the strain-stiffening property of the ECM (page 4).

(b) Upon *compression*, $\lambda < 1$, the fiber buckles. It initially resists its compression, until a critical load is reached where the fiber can no longer resist its compression; the fiber cannot sustain this force and eventually collapses.

(c) For zero force, the stretch of fiber is $\lambda = 1$ which means that the fiber is not deformed.

$\mathscr{W}(\lambda)$ is defined only for positive stretches λ. We exhibit here the graph of this functions including negative stretches, in order to point out that $\mathscr{W}(\lambda)$ is non-convex and thus, we shall expect multiple local minima during the optimization.

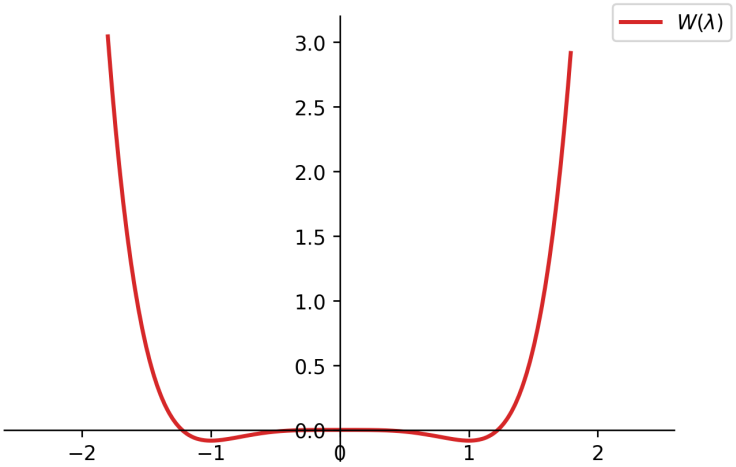

FIGURE 2.16. $\mathscr{W}(\lambda)$

The **total energy** stored in the network is the summation over individual energy-values of all fibers in the network. Let $\mathscr{W}(\lambda_i)$ be the energy of the fiber i, where $i = 1,\ldots,K$, with K to be the total number of fibers in the network. The total energy will be:

$$\mathscr{PE} = \sum_{i}^{K} \mathscr{W}(\lambda_i) \tag{2.23}$$

As cell(s) contract and induce forces in the network, the total energy is changed. We minimize this energy with respect to all positions of the nodes that are free to move, in order to find the conformation of the network that corresponds to a state of minimum energy. In essence, we minimize the above equation (2.23) of $\mathscr{PE}$ over the degrees of freedom of the entire network,

excluding the nodes on the cells' surface. In addition, we also exclude the nodes of the outer boundary of the domain when it is considered fixed (case (ii) on page 34), while for cases it is considered free of forces (case (i)) its corresponding nodes are considered degrees of freedom.

The reference and the deformed length of each fiber (edge) is calculated as the *Euclidean distance* between the position vectors of the nodes it interconnects. Let $\mathbf{p_1}, \mathbf{p_2}$ be the position vectors of two connected nodes, with coordinates (x_1, y_1) and (x_2, y_2), respectively. The strain energy of the fiber connecting them will be given by:

$$\mathscr{U} = k\left(\frac{\lambda^6}{6} - \frac{\lambda^4}{4} - \frac{1}{6} + \frac{1}{4}\right) \tag{2.24}$$

$$\lambda = \frac{L}{l_o}, \qquad L = \sqrt{(x_1 - x_2)^2 + (y_1 - y_2)^2} \tag{2.25}$$

where l_o the reference length of the fiber. Thereby, the energy function of an individual fiber is a function of four variables (degrees of freedom) and shall be minimized in respect to each one of them.
In general, this means that the total energy of the network, equation (2.23), is a function of $N = 2 \times n$ variables, with n to be the total number of nodes that are free to move, thereby N degrees of freedom for the minimization problem. The minimization algorithms perform a number of iterations in order to converge. To speed up the process, we provided the gradient of the model's energy function. At each iteration, the gradient is calculated as a vector containing the partial derivative of each one of the energy's variables, i.e. the partial derivatives of the degrees of freedom vector $\mathbf{x}$, with respect to each one of its components:

$$\min_{\mathbf{x}} \mathscr{PE}(\mathbf{x}) \tag{2.26}$$

$$\mathscr{PE}(\mathbf{x}) = \mathscr{PE}(x_1, x_2, x_3, \ldots, x_N), \quad i = 1, 2, \ldots, N, \quad \text{N: degrees of freedom} \tag{2.27}$$

$$\nabla\mathscr{PE}(\mathbf{x}) = \left(\frac{\partial\mathscr{PE}(\mathbf{x})}{\partial x_1}, \frac{\partial\mathscr{PE}(\mathbf{x})}{\partial x_2}, \ldots\right) = \frac{\partial\mathscr{PE}(\mathbf{x})}{\partial x_i}, i = 1, 2, \ldots, N, \quad \text{N: degrees of freedom} \tag{2.28}$$

If, for example, we want to calculate the partial derivative of equation (2.27) with respect to x_1, combining (2.24) and (2.25) we shall have:

$$\frac{\partial\mathscr{PE}(\mathbf{x})}{\partial x_1} = k\frac{(x_1 - x_2)}{l_o \cdot L}(\lambda^5 - \lambda^3) \tag{2.29}$$

where x_2 is taken as constant, since the derivative has been taken with respect to x_1.

2.5.3 Software

The model was developed using the Python programming language (Python Software Foundation, `https://www.python.org/`) and the finite element software FEniCS (FEniCS Project, `https://fenicsproject.org/`) .

CHAPTER 3

RESULTS

The current chapter includes the results of our simulations. For each case we note the significance of the findings being in accordance or in contrast, to previous models and experimental studies.

3.1 Initial simulations

In section (2.1) of Chapter I, we introduced the *Deformation Gradient* $\mathbf{F} = \nabla\mathbf{f}(\mathbf{x})$ of a mapping $\mathbf{f}$, as well as its *Jacobian Determinant*, $\mathscr{J}$, defined as the local volume ratio of the transformed volume devided by the reference volume of a small region around particle with reference position vector $\mathbf{x}$.
Specifically in our two-dimensional triangularized domain, $\mathscr{J}$ is computed for each triangle separately and refers to the ratio of the area that a triangle occupies in the deformed configuration, to its reference area:

$$\mathscr{J}_i = \frac{T_i'}{T_i} \tag{3.1}$$

where T_i', T_i the deformed and reference area, in respect, of triangle i.
If the Jacobian determinant of a triangle i is positive, then the deformation f preserves orientation; if it is negative, f reverses orientation.
The absolute value of the Jacobian determinant gives us the factor by which a deformation f expands or shrinks areas. Thereby, it can be used to quantify local deformations induced in the fiber networks. In particular, we illustrate the deformed fiber networks according to the $\mathscr{J}$ ratio of each element(triangle). This representation also helps us to identify elements that reversed their orientation, leading to interpenetration and, by that, explore ways to revise this phenomenon.

We start by presenting simulations of one cell with radius $\alpha = 2$, embedded in a domain of radius $A = 10$. We discriminate two cases for which the resolution of the domain is 30 and 40, respectively (Fig. (3.1)). We simulate the cell's contraction, by imposing radial displacement $u_o = -1.0$ at its boundary-nodes. This means that the cell reduces each initial radius by half. The outer boundary of the domain is *free*, i.e. no boundary condition is imposed.

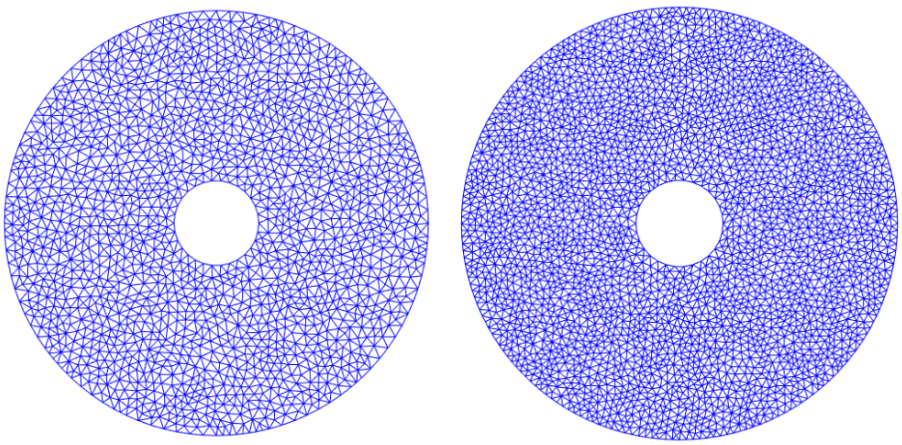

FIGURE 3.1. Networks with resolution 30, left, and 40 right. The domain has radius $A = 10$ and the cell $\alpha = 2$ before contraction.

Upon cell's contraction, the deformations induced lead to interpenetration of some of the elements within the network as depicted below:

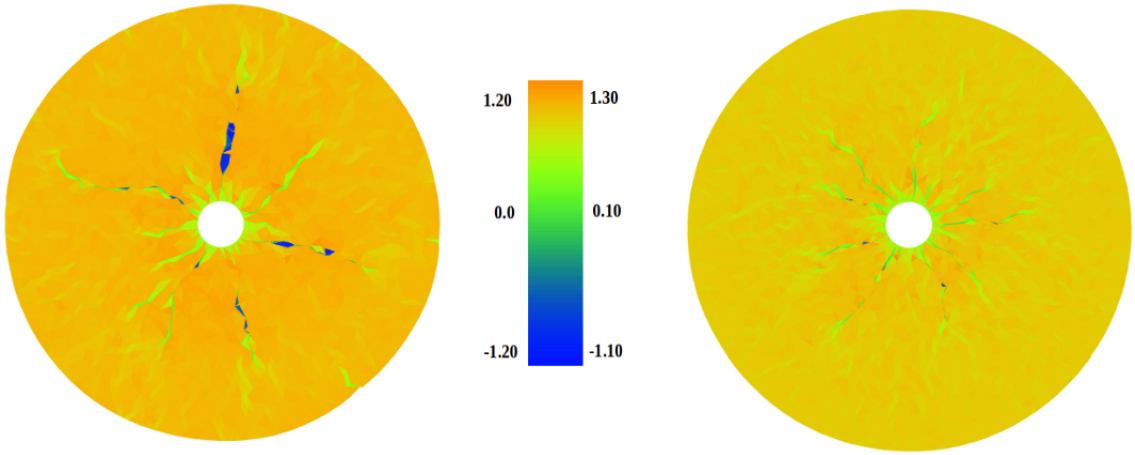

FIGURE 3.2. Equilibrium states of the network after cell's contraction to 50 % of its initial radius. The networks are coloured based on the ratio of area of each triangle, $\mathcal{J}$. Both of them include elements that have changed orientation, i.e. triangles with *negative* $\mathcal{J}$ (blue regions) ***Left*****:** resolution = 30, ***Right*****:** resolution = 40

Interpenetration resulted also in simulations of networks with two contractile cells. This phe-

nomenon is not physically acceptable, as we have already discussed. In the following section we present how we penalized this behavior. After the penalty was induced, we implemented methods in order to validate that the simulations were carried out accurately and that there were no mistakes in calculations regarding the energy and the gradient during the algorithm's iterations. These methods are presented in Appendix.

3.1.1 Interpenetration

The goal was to prevent a possible change in orientation of elements in the network. During minimization, the algorithm seeks the proper rearrangement of nodes, so that the total energy of the network is less than it was in previous iterations. Elements penetrate each other because their corresponding nodes are rearranged in a way that minimum energy is reached. The main idea, is to add a *penalty* in the Energy function, so that the latter takes higher values when an inappropriate rearrangement is reached and thereby force the algorithm to ignore the current solution and search in directions that lead to physically acceptable rearrangement of the nodes.

The penalty is essentially a function added to the total energy of the network and it has to be chosen in a way that it increases the system's energy only when nodes occupy positions that lead to interpenetration. In all other cases, i.e. rearrangements that do not cause changes in orientation, this function should not contribute to the total energy at all.

Considering this restriction, as well as the fact that the factor associated with the orientation is the Jacobian Determinant $\mathscr{J}$, the penalty is formulated as a function $\Phi(\cdot) \in C^1$*, with the property of penalizing $\mathscr{J}$ when this tends to zero, under the conditions:

(i) For very small values of $\mathscr{J}$ close to zero, $\Phi(\mathscr{J})$ should take very large values, and

(ii) For bigger positive values of $\mathscr{J}$, $\Phi(\mathscr{J})$ tend to zero, so that it does not contribute to the total energy of the network.

Let a network contains M triangles, then $\Phi(\mathscr{J})$ is calculated for each triangle m, $m = 1,\dots,M$, in the network. So that the system's energy, equation (2.27), is redefined as:

$$\mathscr{PE} = \sum_{i}^{K} \mathscr{W}(\lambda_i) + \sum_{m}^{M} \Phi(J_m) \qquad i = 1,2,\dots,K \text{ fibers and } m = 1,2,\dots,M \text{ triangles} \tag{3.2}$$

where the first term refers to the system's energy, as a sum over the individual fibers' energies, and the second term corresponds to the sum over all the individual penalty $\Phi(\cdot)$ values of all triangles.

*A function f is said to be of class C^k if the derivatives f', f'',…, $f^{(k)}$ exist and are continuous.

Taking into account the aforementioned conditions (i),(ii), we seek for a formula that grows exponentially for very small values of $\mathscr{J}$, and for that we explored the following:

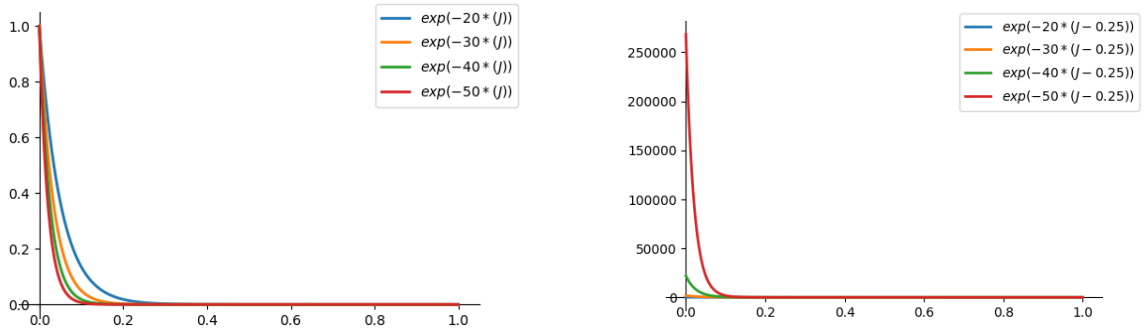

On the left we present the multiple factors used to steep the function's slope, so that it grows for values of $\mathscr{J}$ very close to zero. We see that $\Phi(\mathscr{J}) = exp(-50\mathscr{J})$, red curve, grows more abruptly in contrast to others. In addition, if we add an extra term in the exponent, red curve on the right, $\Phi(\mathscr{J}) = exp(-50(\mathscr{J} - \frac{1}{4}))$, we see that the penalty exhibits exactly the desired behavior; very close to zero it grows abruptly to very large numbers, otherwise it tends to zero.
Furthermore, since we developed networks of different resolutions, we suggest that the penalty term should not depend only to the ratio $\mathscr{J}$, but to the ratio with respect to the initial area that a triangle occupies. So that the penalty function is finally formulated as:

$$\Phi(J) = A \cdot \exp(\alpha(J + \beta)), \quad \alpha = -50, \quad \beta = -\frac{1}{4} \tag{3.3}$$

and then equation (3.2) becomes:

$$\mathscr{PE} = \sum_{i}^{K} \mathscr{W}(\lambda_i) + \sum_{m}^{M} A_m \cdot \exp(-50(J_m - \frac{1}{4})) \tag{3.4}$$

where K is the total number of fibers in the network, M the total number of triangles, $\mathscr{W}(\lambda_i)$ the potential energy of an individual fiber, A_m the reference area that triangle m occupies and $\mathscr{J}_m$ the ratio of its deformed to its reference area.

Remark: The derivative of $\mathscr{PE}$, equation (2.29), should also be updated, since the Jacobian $\mathscr{J}$ is derived from a triangle's area, which in turn is defined by the position vectors of the nodes that determine it. This calculation is presented in Appendix section.

After the penalty was induced, the simulations regarding the networks with one contracting cell in resolutions 30 and 40, Fig. (3.2), resulted in:

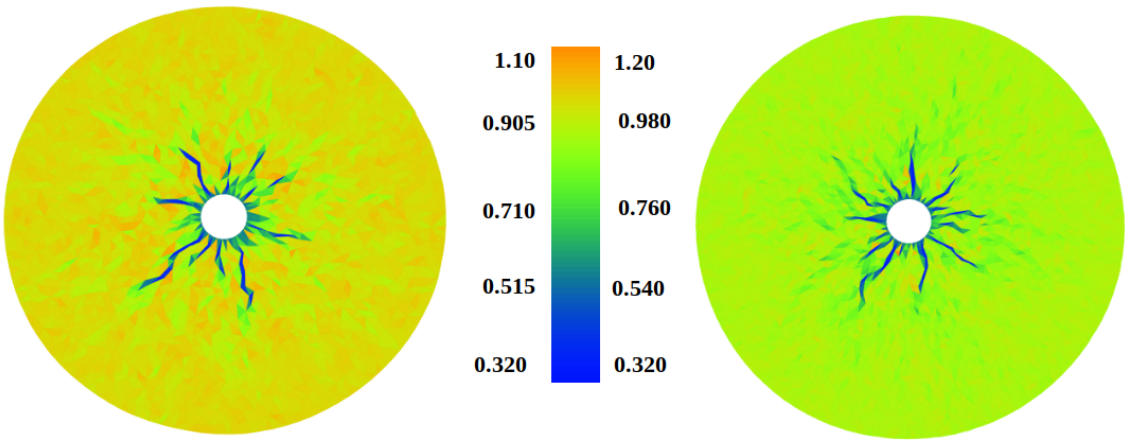

FIGURE 3.3. Interpenetration is successfully prevented. The equilibrium states of the networks in Fig. (3.2) do not include elements with reversed orientation. The networks are coloured based on the ratio of area of each triangle, $\mathscr{J}$, which is strictly positive everywhere. ***Left*:** resolution = 30, ***Right*:** resolution = 40.

We managed to penalize successfully the interpenetration in our networks. In the figures above we observe that the blue areas correspond to highly compressed triangles but the Jacobian is positive. For the rest of our analysis simulations have been performed using equation (3.4) of the updated energy function.

3.2 Cell-induced matrix displacements

In this section we present results regarding networks of one contracting cell. The aim is to explore how the matrix deforms following a cell's contraction, as well as the propagation of the induced displacements.
We begin by examining the latter case we previously saw, with one cell of radius $a = 2$ embedded in a domain of resolution 40 and a traction free outer boundary. The cell contracts uniformly by $u_o = -0.5 \cdot a$, reducing its radius in half:

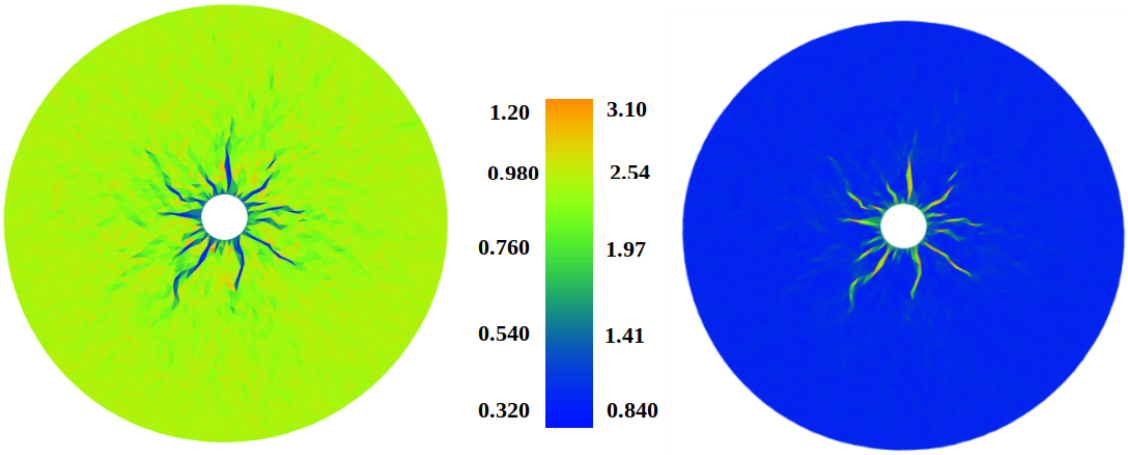

FIGURE 3.4. Cell contraction to 50% of each radius. ***Left*:** Network is coloured based on the Jacobian determinant of each triangle. ***Right*:** Network's area density normalized by its reference area density.

Let us examine these two figures. On the left, we have the deformed network where each triangle is colored based on the Jacobian determinant value. In particular, we focus on the *blue areas* which correspond to *highly compressed triangles* ($\mathcal{J} << 1$). On the right, we present the networks's **area density**, calculated for each triangle separately and normalized by their reference density. We see that the **blue areas of highly compressed triangles**, from the figure on the left, **correspond to regions of high density**.

These highly densified regions are formed because the **corresponding triangles nearly collapse due to buckling of some of their fibers**.

This statement is better explained in the following configurations where we initially present the network in its deformed state and then the tensile and compressed stretches of the deformed network, separately:

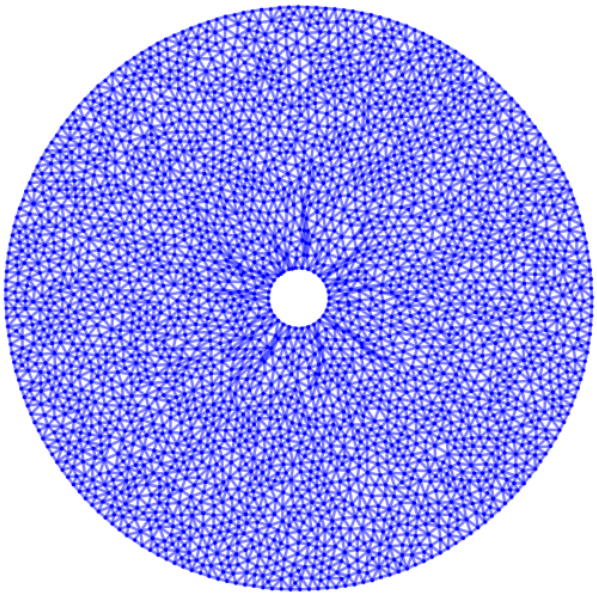

FIGURE 3.5. Deformed configuration of the network.

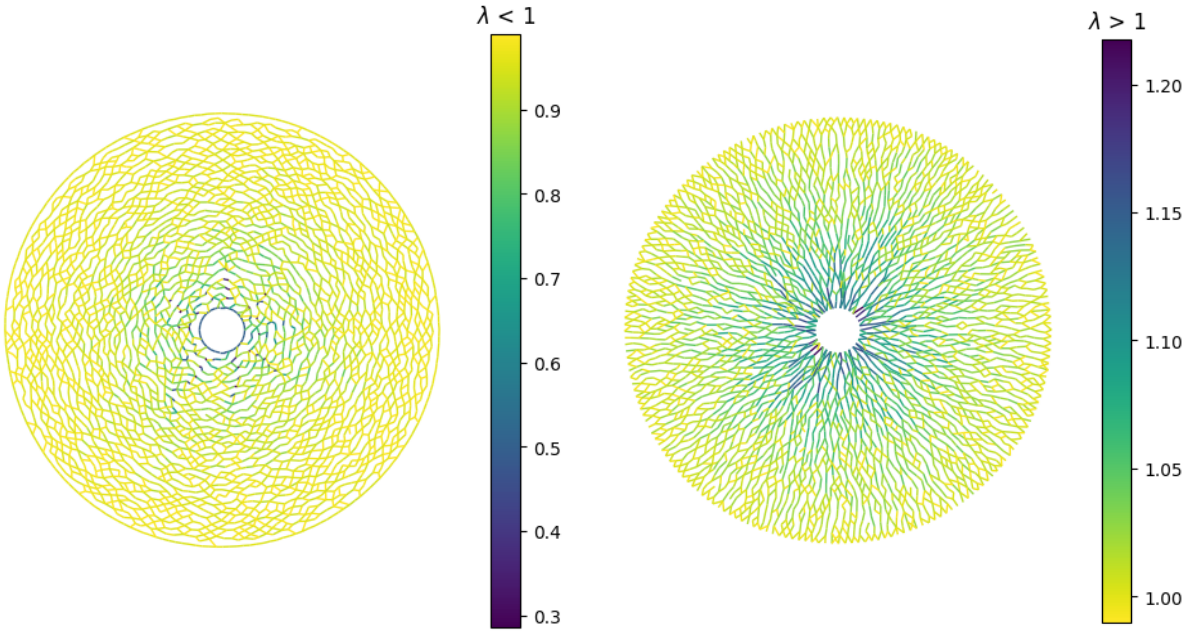

FIGURE 3.6. Compressive and tensile strains of fibers. ***Left*:** Compressive stretches, $\lambda < 1$ of fibers oriented in the angular direction. ***Right*:** Tensile stretches, $\lambda > 1$, of fibers oriented in the radial direction.

If we focus on the area around the cell, in Fig. (3.5) and in the compressive stretches of Fig. (3.6) we clearly see that the highly densified regions we observed in Fig. (3.4) are indeed regions where triangles collapse due to highly compressed fibers that buckle (dark blue stretches, in Fig. (3.7) on the right) :

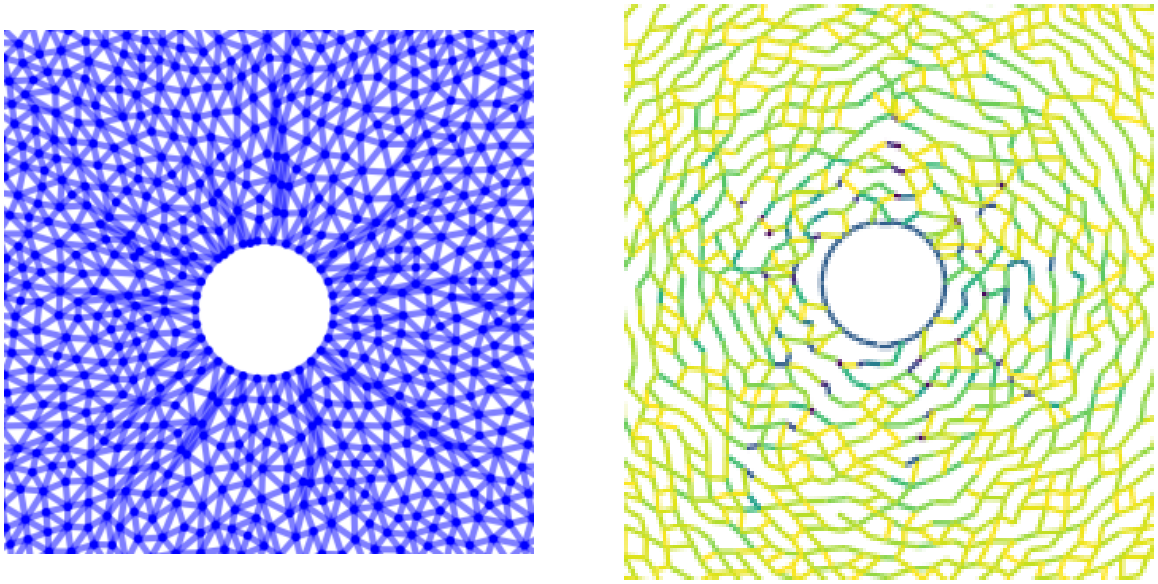

FIGURE 3.7. Highly densified regions around the cell are formed due to fibers that buckle under compression. ***Left*:** Deformed state of network with focus on the compressed triangles around the cell. ***Right*:** Compressive stretches of the network, with focus again on the same regions. The triangles that are highly compressed consist of fibers that buckle (dark blue stretches).

We double the resolution of the network above, from 40 to 80. By doing so, the reference fiber lengths are reduced by half (more on page (50)). This increases the network's thickness. And, as we see below, in a more thick network we spot many more densified regions around the cell, compared to the the network of 40 resolution:

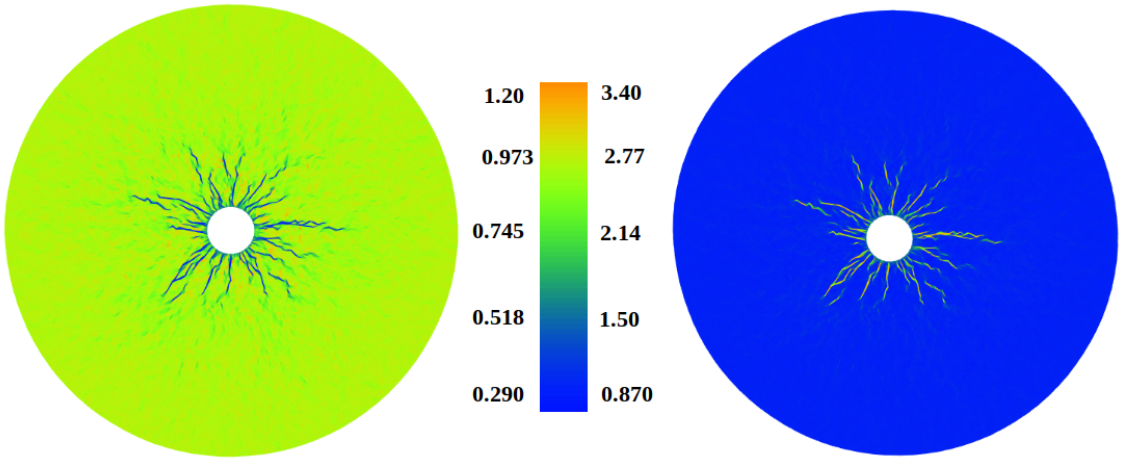

FIGURE 3.8. Network of resoltion 80 and cell contraction by 50% of its radius. ***Left***: Network is coloured based on the Jacobian determinant of each triangle. ***Right***: Network's area density normalized by its reference area density.

The densified regions around the cell are formed due to fibers that buckle under compression, as we saw before. In addition, in this thicker network we observe the following:

i. These hair-like regions are *irregular* and not straight.

ii. They are also *interrupted* and not continuous.

Stopak and Harris in [33] studied the distortion of the extracellular matrix due to cells' contractility. Following, we reproduce a figure of a ganglion consisting of several cells that contract. At a low magnification such this, the cells cannot be distinguishable. The bright body in the center corresponds to the ganglion and the bright wavy lines that surround it are *wringles*, the result of the deformation induced by the cells which constitute the ganglion. By comparing this figure with the area density plot above, Fig. (3.8, right), we see that the hairs around the simulated cell resemble the wrinkles observed in the experiment. Wrinkles are interrupted and wavy (not straight), in accordance to what we clarified above regarding the simulated hairs.

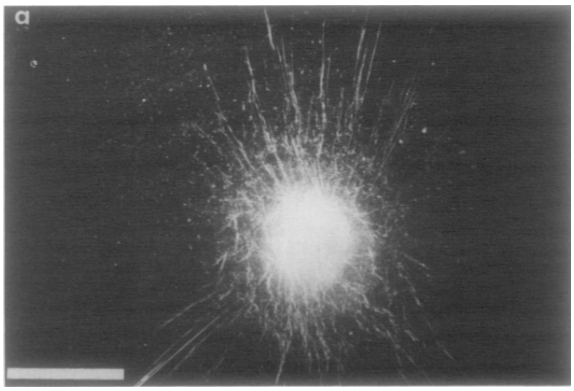

3.3 Decay of displacements

Previously, we investigated how a single contracting cell deforms its surrounding space and how buckling of compressed fibers contributes to these deformations. In this section, we explore how far displacement fields propagate far from the contracting cell.

Consider a network of resolution 40 with one contracting cell, just like the ones we investigated previously. We depict on the right the **displacement field** in the network after the cell's contraction which shows different ranges of displacement magnitudes along the disk. In particular, displacements are largest near to the cell and decrease with distance from it:

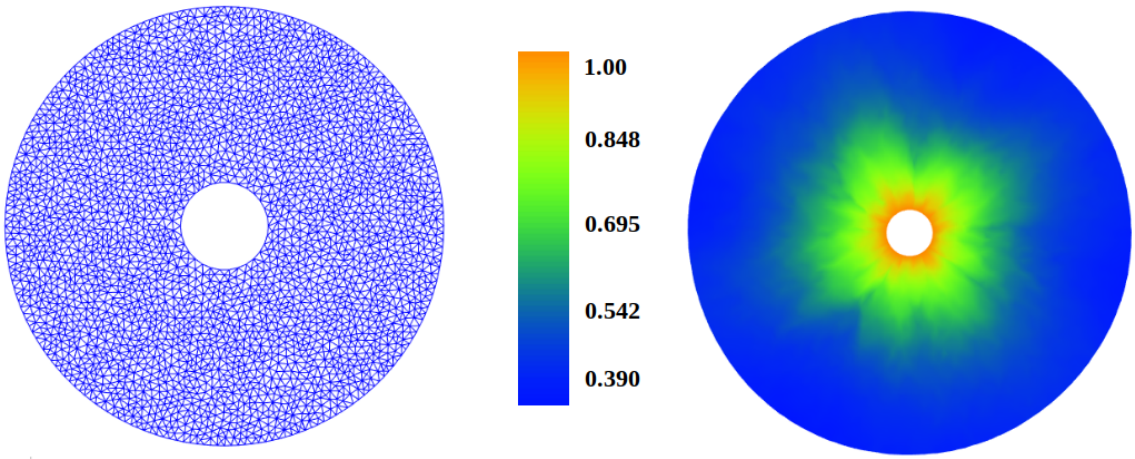

FIGURE 3.9. Cell contraction to 50% of each radius. ***Left*:** The reference domain of resolution 40 and radius $A = 5a$, where $a = 2$ is the cell's radius. The maximum fiber length for this network is $hmax = 0.5$ and $hmin = 0.25$. ***Right*:** Contours of the displacement magnitude **u**.

It is essential to explore how fast or slow these displacements decay. This will provide us a quantification of the displacements propagation over the disk and thereby an insight of cell's zone of influence. The propagation of displacements induced by a contracting cell facilitates the mechanism of cell mechanosensing and cell-cell communication, rendering its exploration as high important.

Notbohm *et al.,* 2015 in [23] and Burkel in [4, 5], make use of a power law provided by Linear Elasticity in order to quantify the decay of displacements induced by one contracting cell. In particular, they fit experimental data, as well as simulated displacements, to the form:

$$u(r) = Ar^{-n} \tag{3.5}$$

where $u(r)$ is the radial component of displacement, r is the distance from the center of the contracting cell and A, n are constants with $n > 0$ to be the **decay power**.

We discriminate the following:

i. Larger n: displacements decay **faster** with distance r from the center of the cell.

ii. For smaller n: the displacements **propagate in longer range** from the center of the cell.

Linear Elasticity predicts that in a linear elastic material the displacements decay with order $O(r^{-2})$ in three dimensions and with order $O(r^{-1})$ in two dimensions.
We fit the resulted displacements of our simulations in equation (3.5), and in addition, for extra exploration and validation, to the equations:

$$\begin{aligned} u(r) &= Ar^{-n_1} + Br \\ u(r) &= Ar^{-n_1} + Br^{n_1} \\ u(r) &= Ar^{-n_1} + Br^{n_2} \end{aligned} \tag{3.6}$$

The first one corresponds to the general solution of Linear Elasticity while the second is similar to equation (3.5) but with an added second term, proposed by Rosakis *et al.,* 2015 in [26] and used by Notbohn and Burkel in [23], [5], respectively, in addition to equation (3.5). The last equation is a generalized form of the second one.
Accordingly, we fit the simulated radial displacements of the nodes in our network, normalized by the radius a of the cell, in each one of the aforementioned equations. We have the following:

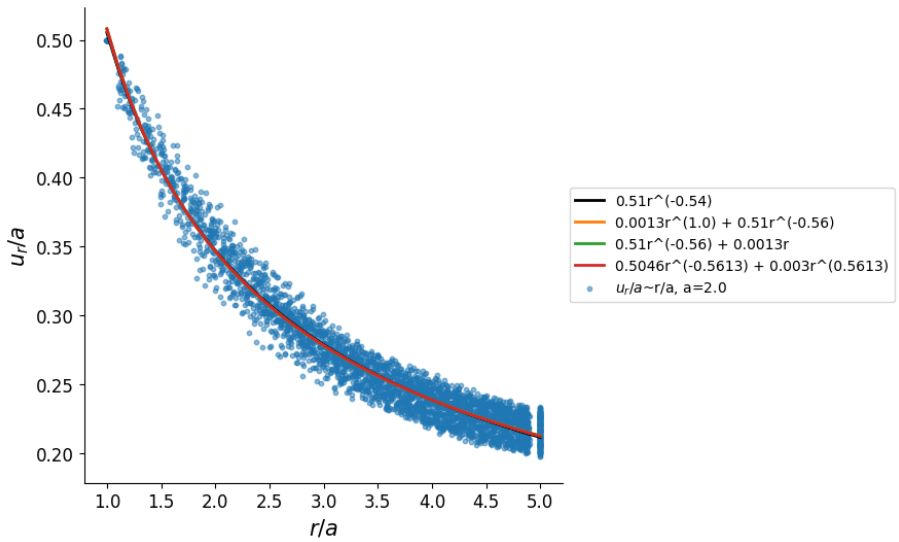

FIGURE 3.10. ***Blue dots*:** Normalized radial displacements for all nodes plotted against their corresponding distance r from the center of the cell. ***Fit curves*:** Fits of each one of the presented equations which coincide, as the value of the fitting parameter n is very similar for the different fits.

The black line corresponds to the Ar^{-n} fit, the orange to $Ar^{-n_1} + Br^{n_2}$, the green to $Ar^{-n_1} + Br$ and the red one to $Ar^{-n_1} + Br^{n_1}$. We see a total agreement between the orange and the green

fit, with parameter $B \approx 0$ in both of them and $n \approx 0.56$. In addition, in the red fit $Ar^{-n_1} + Br^{n_1}$ parameter $B \approx 0$, while $n \approx 0.56$ so that the fit agrees to the previous ones. The decay power $n \approx 0.56$ is very close to the first fit Ar^{-n_1} where $n \approx 0.54$.
In any case, this value for the decay power n indicate that *displacements decay much slower than predicted by classical linear theory, where* $n = 1$ [23, 26]. The long range propagation of displacements in our networks agrees with previous experiments [4, 23, 37] where contracting cells were observed to produce displacement fields that propagated over a long range. In addition, **the decay power $n \approx 0.56$ validates that our model of fiber buckling captures the long-range propagation of displacements induced by o contracting cell.** Thereby, buckling is a key mechanism for the longer-range of cell-induced deformations in a fiber matrix.

Following, we check whether the magnitude of cell's contraction affects the decay of the induced displacements. Therefore, we simulate cell's contraction with radial contractile displacement equals to $15\%, 25\%, 35\%$ and 50% of the cell radius ($a = 2$), in a network of radius $A = 5a$.
We see that decay power n decreases as the contraction of the cell increases. Thereby, **greater contractions result in longer propagation of displacements in the network.** This dependence on cell's contraction is a result of the nonlinear relation in force-stretch for fibers under compression and is in contract to previous studies, [23, 26], which state that cell's contraction does not inlfuence the propagation of induced displacements.
Finally, we also note that simulations with networks of different resolutions (20, 40, etc.), but with the same radius A, resulted in similar decay power n.

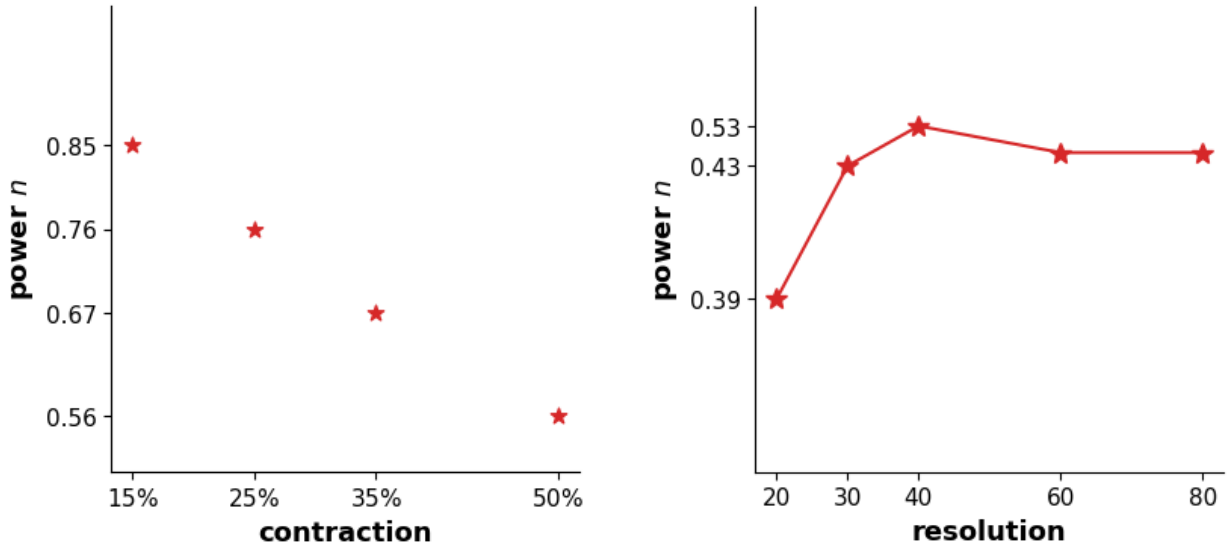

FIGURE 3.11. ***Left*:** Different levels of a cell's contraction affect the decay of induced displacements. ***Right*:** Induced displacements in networks of same radius A and different resolutions propagate in a similar way.

3.3.1 Reduced Connectivity

Another important aspect of fiber networks is their *connectivity* which refers to the average number of fibers meeting at a node. A typical network of our models, like the one in Fig. (3.9, left) has connectivity $C \approx 6$. In order to obtain networks with lower connectivity, we remove fibers (edges) by setting their stiffness constant equal to zero. The choice of fibers to be removed occurs in a random yet controlled manner in order to avoid cutting all edges coming through the same node.

In particular, we discriminate three cases; at each case, we remove one, two or three fibers of each node respectively. So that in each case the network reduces its connectivity to approximately 4.74, 3.7 and 2.87 average number of fibers at each node with a standard deviation 1.10, 1.15 and 1.09 respectively.
We perform simulations for these different connectivities and investigate the decay of induced displacements. The networks have radius $A = 5a$, where a is the cell's radius, and the cell undergoes a radial contractile displacement of $u_o = -0.5a$, i.e. reducing each area in half. Below, we present the fits of $u(r)$ to equations (3.5 - 3.6) for each one of the connectivites 4.74, 3.7 and 2.87. The initial (full network) $C \approx 6$ has been explored above, Fig. (3.10). So for each one of the reduced connectivities, we have in turn:

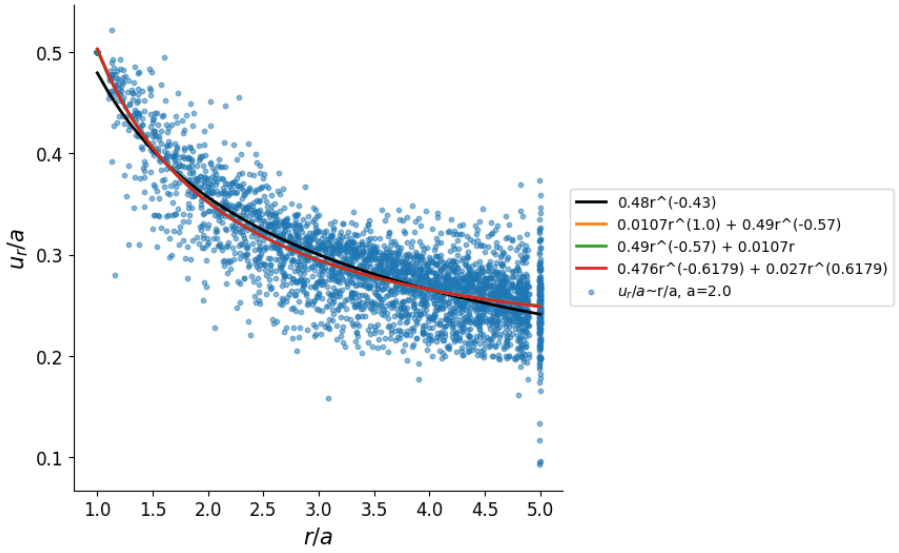

FIGURE 3.12.

C ≈ 4.74 : We see that in this case, power n is the same for the two of the fits, orange and green curves, but deviate from the other two, even though it is close to power n of the red curve fit. In any case, n is again below $n \approx 1$ of the elastic solution.

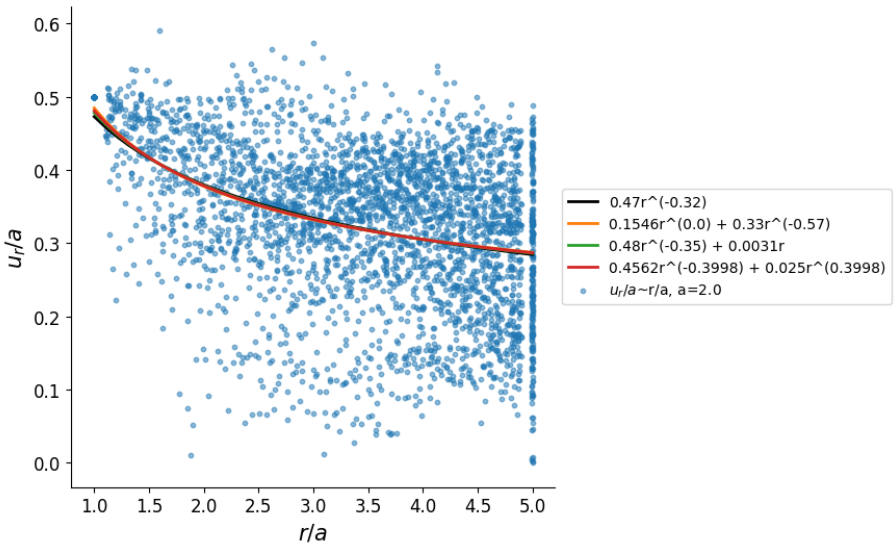

FIGURE 3.13.

C ≈ 3.7 : Same behaviour as above. Power n shows a small deviation among the different fits, but remains below one in all cases. We note that displacements in this network are much more scattered in contrast to the previous network of $C = 4.74$ and to the one with full connectivity, $C \approx 6$, in Fig. (3.10). We also observe that nodes on the boundary have various magnitudes of radial displacements compared to previous networks, where nodes on the outer boundary have a radial displacement of magnitude in the range 0.2 to 0.4.

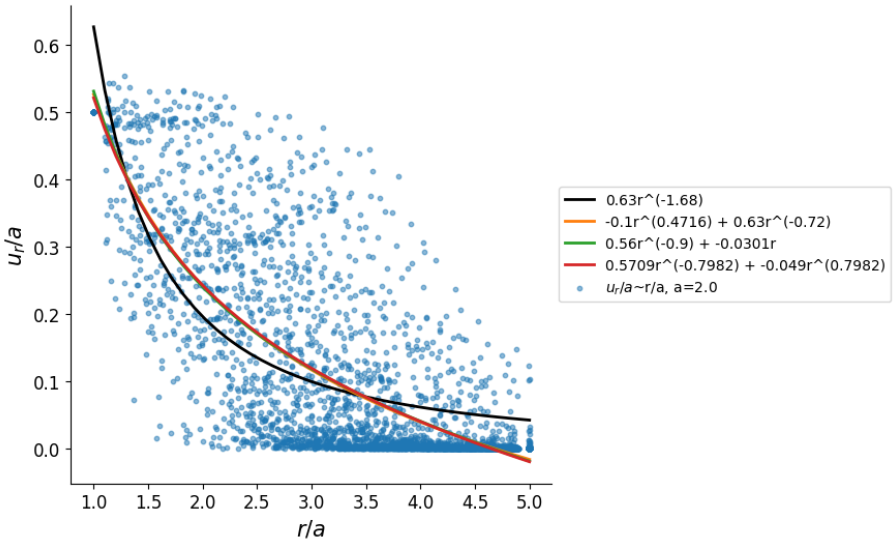

FIGURE 3.14.

C ≈ 2.8 : For this connectivity, the decay of displacements is closer to the elastic solution, as all fits have power n close to elastic solution 1. In this network, we observe that many nodes in various distances from the cell center, r, do not move at all.

We note that for the latter connectivity $C \approx 3$ the decay power is close to elastic solution, meaning that for this connectivity the displacements do not propagate far from the cell but, on the contrary, decay very fast. This comes in contrast to Notbohm in [23], where the critical value of connectivity for which the decay power deviates from smaller values but rather tends to one, is $C = 4$. In addition, while in their study the highest value of n was reported for $C = 4$, in our simulations for connectivity $C \approx 3.7$ close to 4 the decay power n takes its minimum value compared to all other connectivities.

In previous section, in order to investigate how the induced loads due to cell's contraction deform the fiber network we presented separately the simulated compressive and tensile stretches. We repeat the same for each one of the different connectivities we discussed above. Starting with the stretches for the full connected network ($C \approx 6$) in Fig. (3.15), that we have already presented before and pointed out that tensed fibers (3.15 on right) are observed to straighten, generating linear chains that emanate *radially* from the contracting cell. At the same time, we see compressed fibers (3.15 on left) to be oriented in the *angular* direction. The network with $C \approx 4.74$ exhibits similar behaviour, Fig. (3.16). These observations agree with previous models [23, 30] and experiments [4, 18, 21]. However, in Fig. (3.17) and (3.18) this phenomenon gradually fades as the connectivity of the network is being reduced.

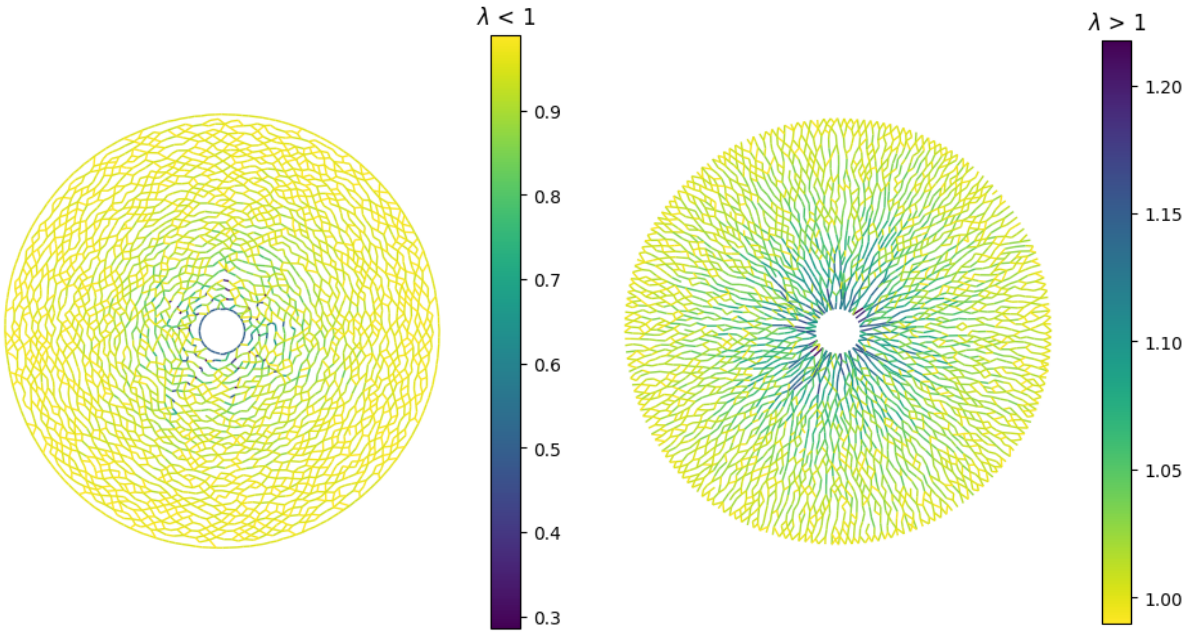

FIGURE 3.15. Compressive and tensile stretches of fibers within the vicinity of a contracting cell, for 50% contraction and full connectivity $C \approx 6$. ***Left*:** Compressive stretches, $\lambda < 1$, of fibers oriented in the angular direction. ***Right*:** Tensile stretches, $\lambda > 1$, of fibers oriented in the radial direction.

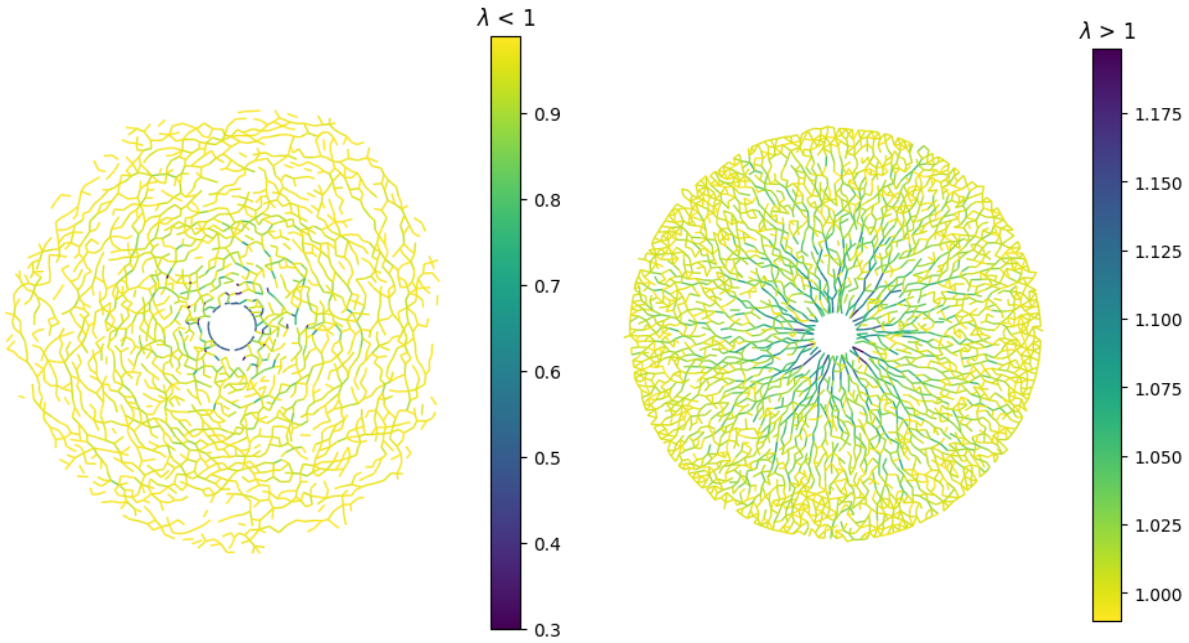

FIGURE 3.16. Connectivity $C \approx 4.7$. ***Left*:** Compressive stretches, $\lambda < 1$, of fibers oriented in the angular direction. ***Right*:** Tensile stretches, $\lambda > 1$, of fibers oriented in the radial direction.

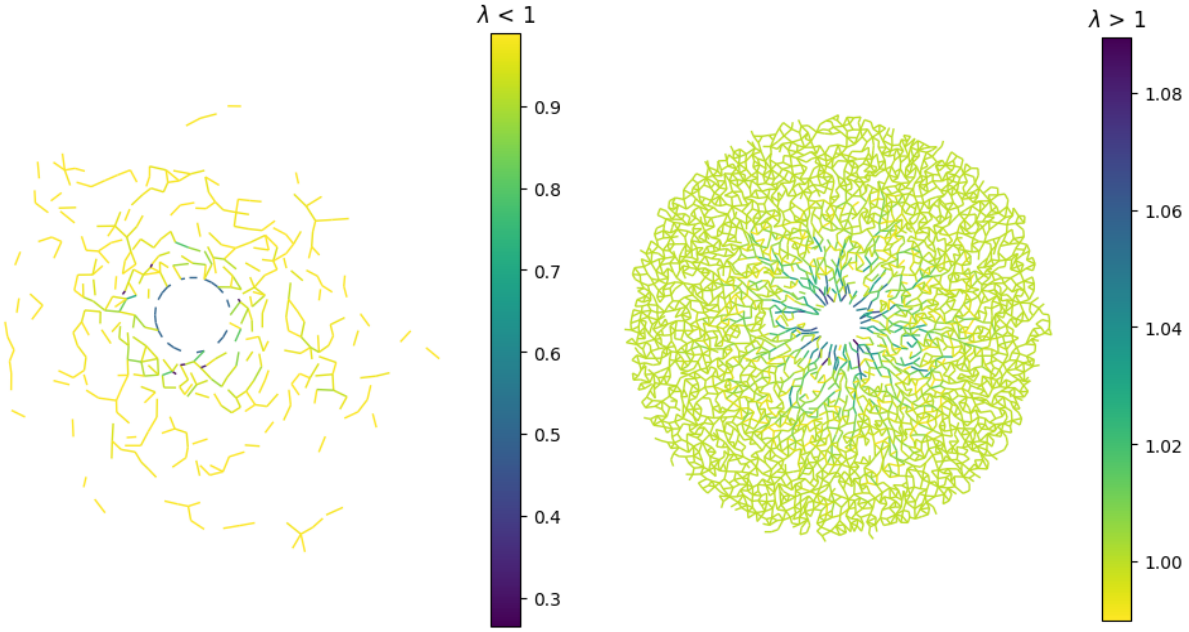

FIGURE 3.17. Connectivity $C \approx 3.7$. ***Left*:** Compressive stretches, $\lambda < 1$, are much less compared to tensile ones on the right figure. We observe that compressed fibers are also oriented in the angular direction, as in more connected networks. ***Right*:** Tensile stretches, $\lambda > 1$, of fibers oriented in the radial direction, most of which lying in the region close to the cell.

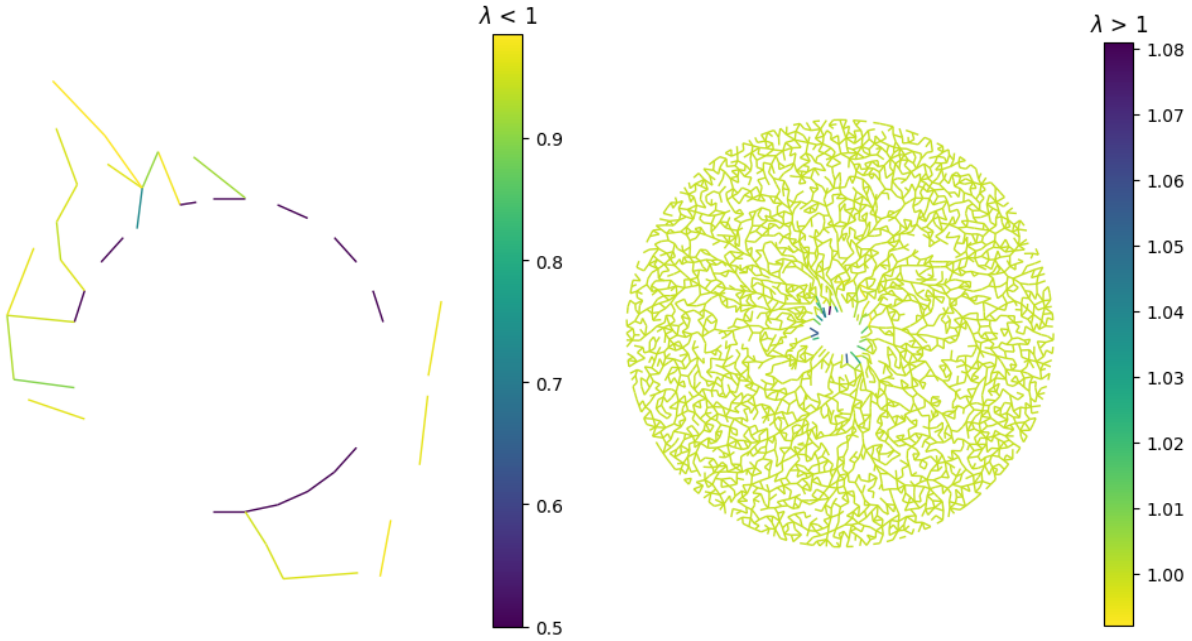

FIGURE 3.18. Connectivity $C \approx 2.8$. Very few compressive stretches, $\lambda < 1$, compared to the tensile on the right.

We observe both the tensile and compressive stetches in the network of $C \approx 3.7$, Fig. (3.17). Especially in the case of tensile stretches, we can see how the observed straighten of fibers in previous networks here fades. Only a few fibers are oriented radially around the cell and they refer to fibers in a small zone of influence around the cell. This zone is even more smaller in the network with the lowest connectivity, Fig. (3.18). We also observe that nodes in this network move in a complete random manner, opposed to how they are rearranged in more connected networks. This is depicted if we compare the reference and deformed domains for this network, Fig. (3.21) with the respective high connected networks in Fig. (3.19) and (3.20). Clearly, we see that nodes are moved along the area of the whole disk, clarifying the big disperse of their radial displacement in Fig. (3.13). It is very interesting to note that moving to the next reduced network of $C \approx 2.8$ we observe the exact opposite phenomenon. Displacements are not so scattered, while there are significantly many ones that remain in their initial positions. In addition, we observe in Fig. (3.18) that there are very few compressive stretches opposed to the tensile ones which are dominant in this network. The decay power for the displacements regarding this network was close to $n \approx 1$, Fig. (3.14), which is close to the elastic solution and corresponds to fast decay of displacements. We note that **in the absence of compressive strains, the network deviates from lower powers of n, indicating that tensile strains, and thereby strain-stiffening, alone cannot facilitate the long range propagation of displacements.**This serves as an extra validation that buckling of fibers under compression is crucial for the slow decay of displacements.

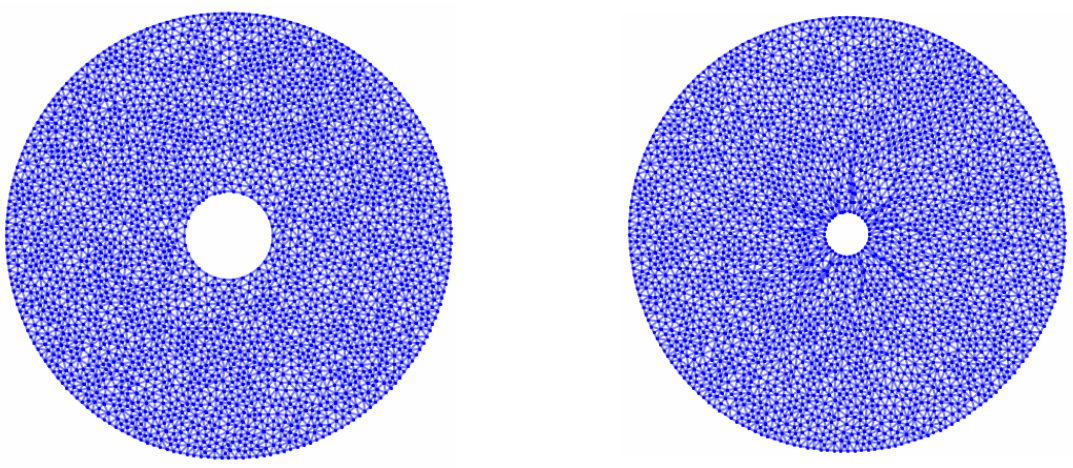

FIGURE 3.19. Full connectivity $C \approx 6$. Reference and deformed domains.

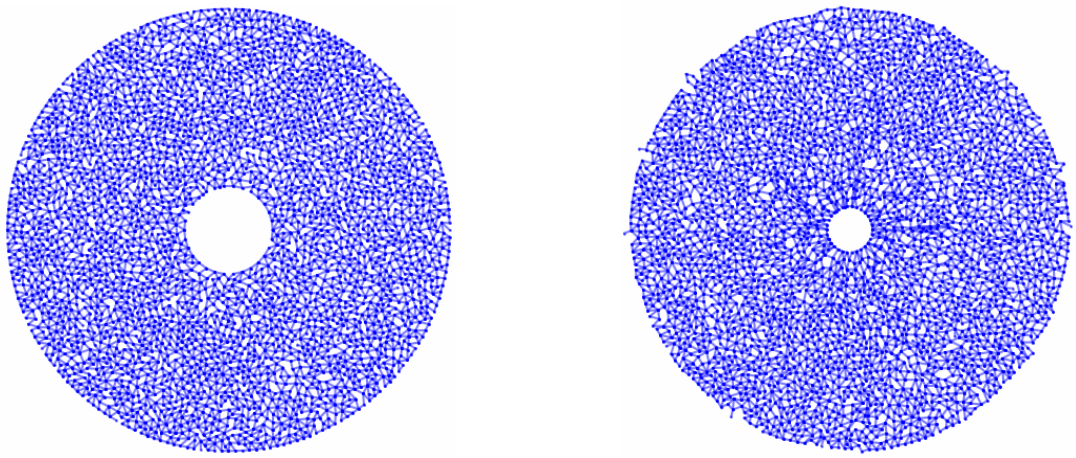

FIGURE 3.20. Connectivity $C \approx 4.7$. Reference and deformed domains.

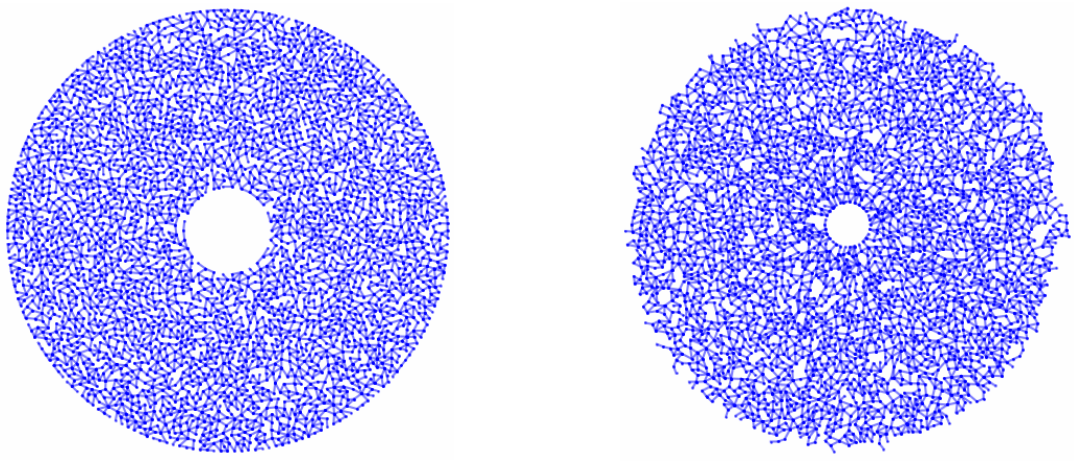

FIGURE 3.21. Connectivity $C \approx 3.7$. Reference and deformed domains.

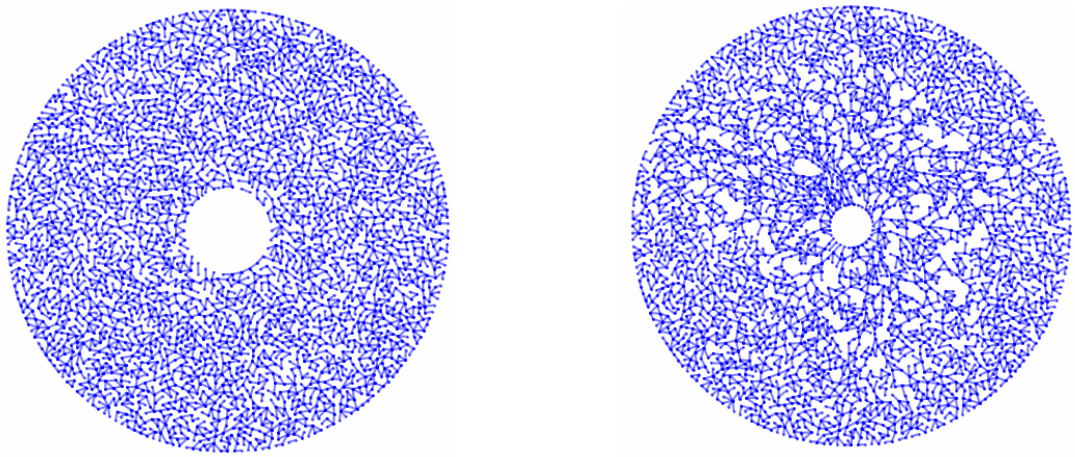

FIGURE 3.22. Connectivity $C \approx 2.8$. Reference and deformed domains.

3.4 Cell-cell interaction

Cells exploit the long propagation of matrix deformations they induce, in order to sense the presence of neighbouring cells. A number of experiments show that neighbouring cells are connected to each other by linear bands consisting of aligned and densely packed matrix fibers [12, 23, 25, 28, 29, 34, 37].

We begin by simulating a pair of two identical cells of radius $a = 2$ embedded in a disk of radius $A = 5a$ with a traction free boundary. The centers of both cells are coincident with the horizontal line passing through the center of the network, and they have a distance $d = 4a$ between them. Both cells contract by 50% of their radius. We present networks of 50 and 100 resolution, starting with the latter.

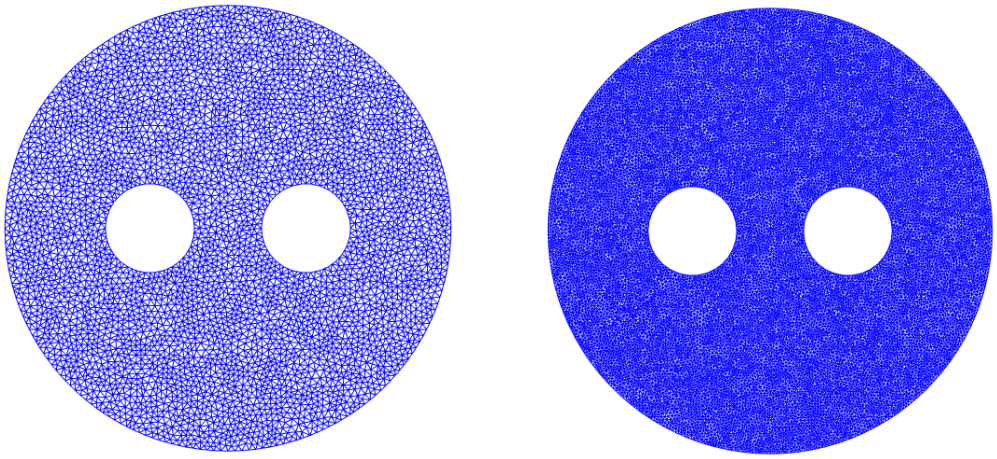

FIGURE 3.23. Reference networks of resolution 50 (left) and 100 (right).

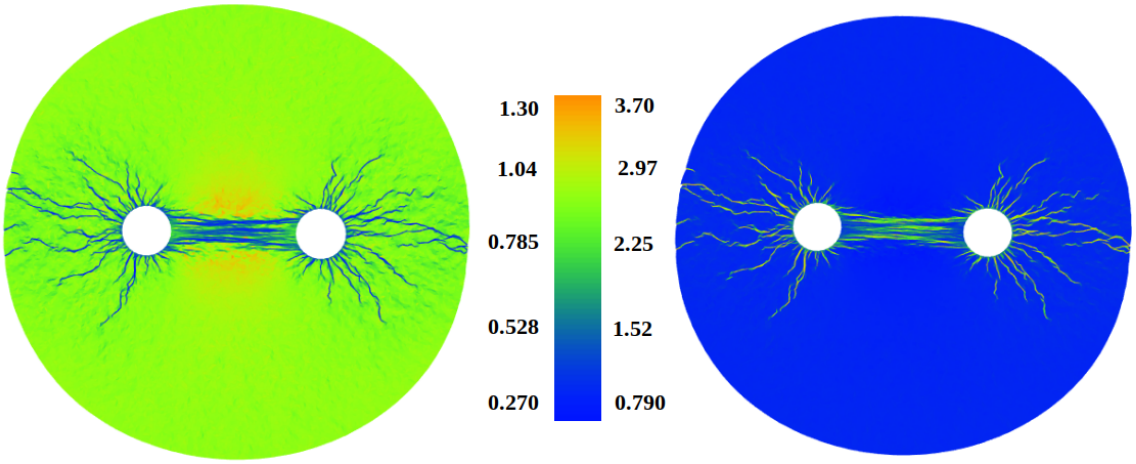

FIGURE 3.24. Band formation between two contractile cells. ***Left*:** The network is coloured based on the ratio $\mathcal{J}$ of each triangle. ***Right*:** The network is coloured based on the area density that each element has in the deformed state after cells' contraction.

Considering the figure of $\mathcal{J}$ we see that the *blue* regions correspond to triangles that have shrunk leading to high densification which is depicted in the density figure. These triangles are located mainly in the inter-cellular region, though we see that they also expand from the periphery of each cell and reach the boundary of the network. With these figures we can quantitatively explore the mechanical interaction between the cells as they provide the local change in the density of the matrix which is a result of the displacements induced by the cells' contraction.
In order to investigate further these regions of higher density and see how fibers' behaviour contribute to the formation of these densed bands, we present the tensile and compressive stretches of the network below in Fig. (3.25). We observe that high tensile stretches occur entirely in the band between the two cells, while the compressive stretches in this region are perpendicular to the tensile ones. We note that the magnitude of the compressive stretches in this region are below $\lambda = 0.5$, corresponding to fibers that buckle. In Fig. (3.26) we focus closely on these regions for better illustration of this phenomenon. In the latter figure, it is easier to discriminate that the tensile strains correspond to straighten and aligned fibers. Thereby the highly dense regions we observed above in the inter-cellular band are indeed facilitated by aligned fibers in tension.

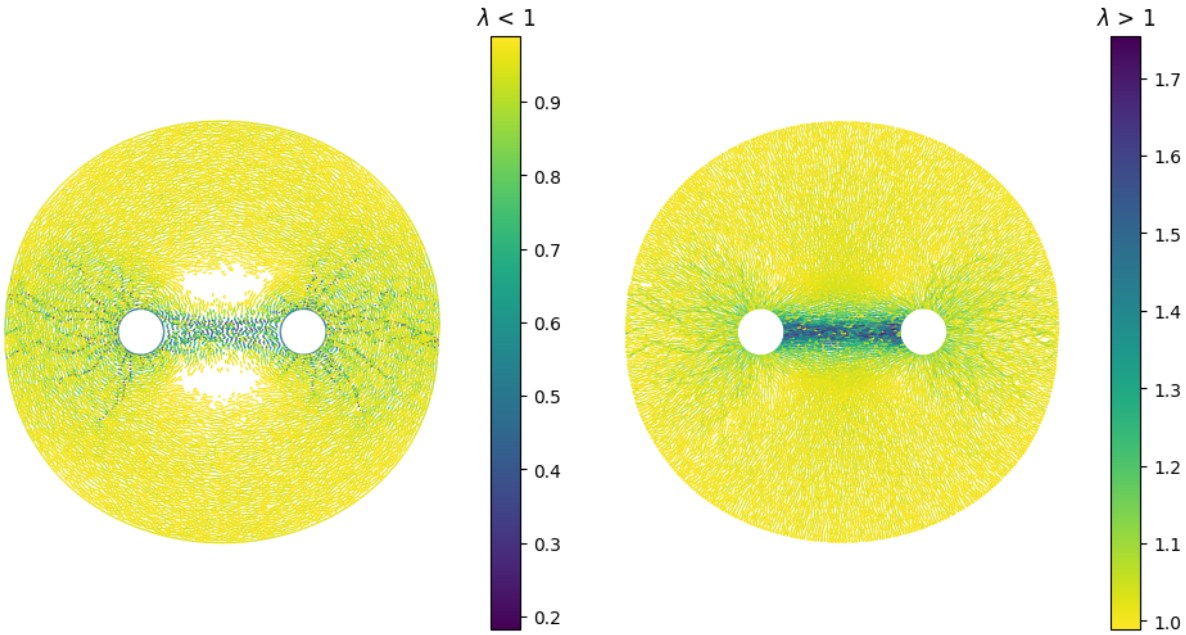

FIGURE 3.25. Compressive and tensile stretches of fibers within the vicinity of the two cells contracting by 50%. ***Left*:** Compressive stretches, $\lambda < 1$, ***Right*:** Tensile stretches, $\lambda > 1$.

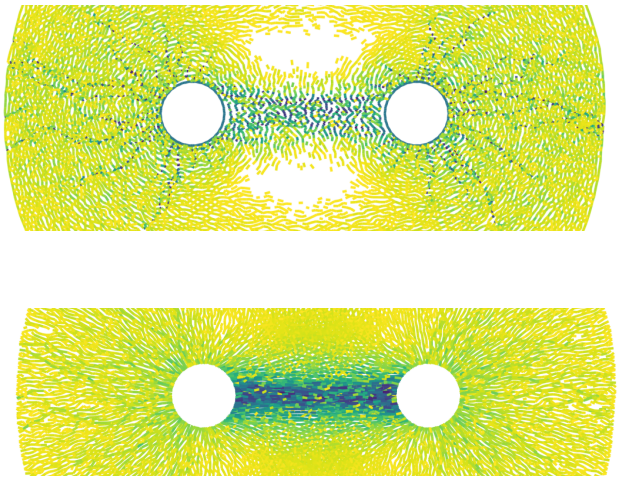

FIGURE 3.26. Compressive and tensile stretches of fibers, focusing on the inter-cellular region. ***Upper*:** Compressive stretches, $\lambda < 1$, ***Lower*:** Tensile stretches, $\lambda > 1$.

A network of resolution 100 is high dense regarding the total number of nodes that it includes and the short reference length of fibers, Fig. (3.23). Thus, we present also the respective results from simulations conducted with a network of resolution 50.

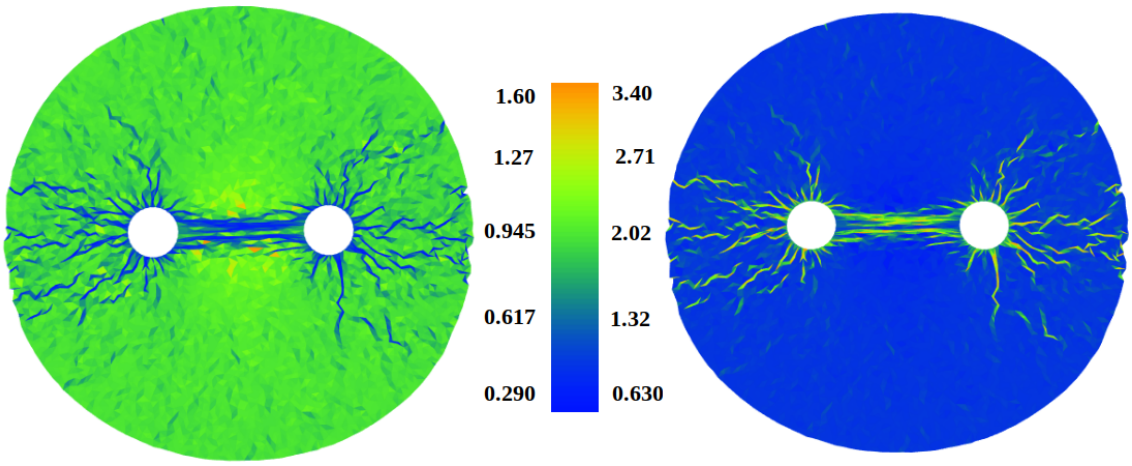

FIGURE 3.27. Band formation between two contractile cells in a network of resolution 50. ***Left*:** The network is coloured based on the ratio $\mathscr{J}$ of each triangle. ***Right*:** The network is coloured based on the area density that each element has in the deformed state after cells' contraction.

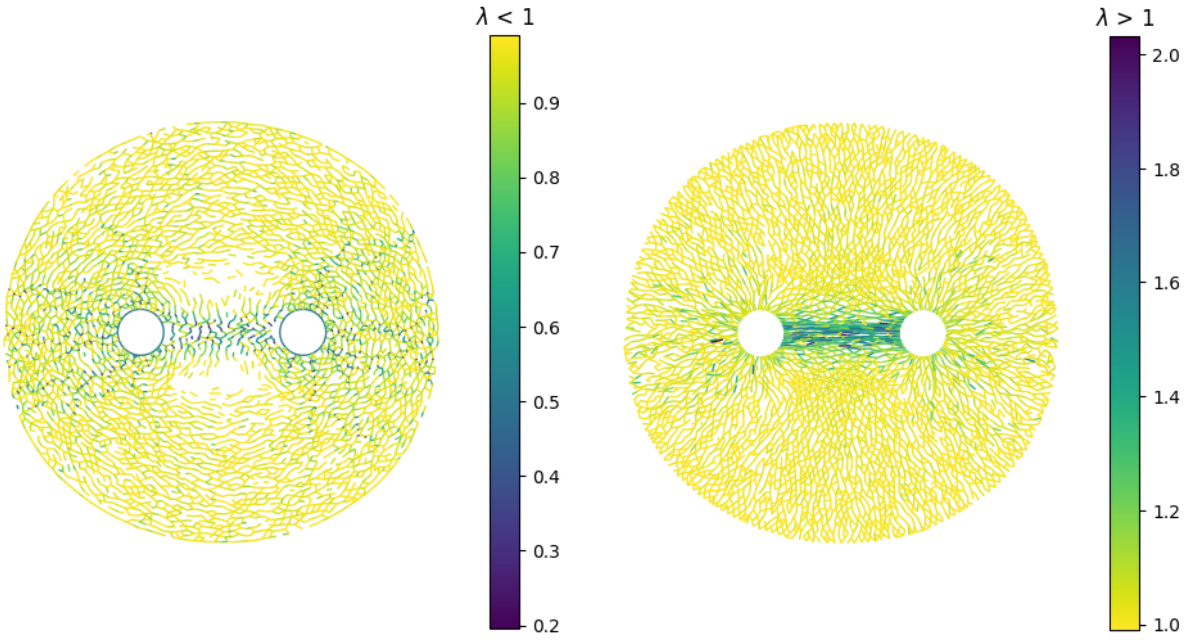

FIGURE 3.28. Compressive and tensile stretches of fibers within the vicinity of the two cells contracting by 50% in the network of 50 resolution. ***Left*:** Compressive stretches, $\lambda < 1$, ***Right*:** Tensile stretches, $\lambda > 1$.

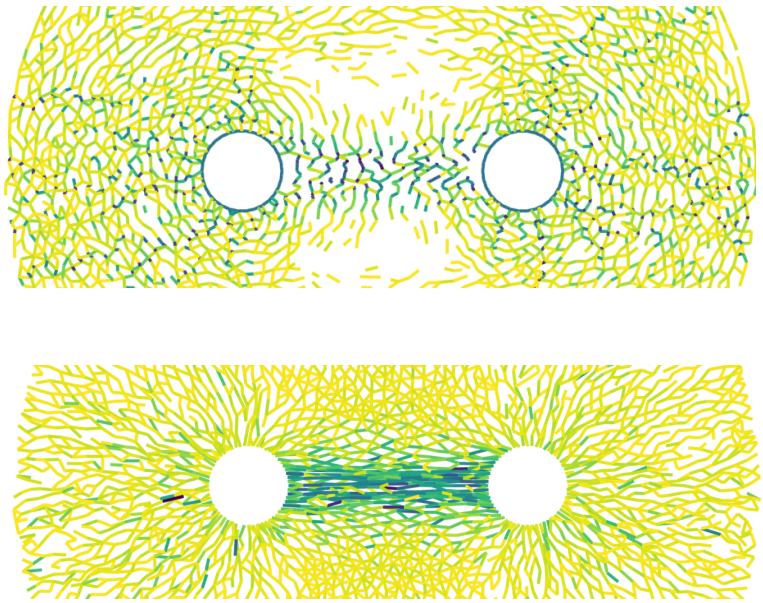

FIGURE 3.29. Compressive and tensile stretches of fibers, focusing on the inter-cellular region. ***Upper*:** Compressive strains, $\lambda < 1$, ***Lower*:** Tensile strains, $\lambda > 1$.

For this network is easier to discriminate the tensile stretches in the inter-cellular region forming bands of aligned linear paths while the compressive ones being perpendicular to the tensile. Bringing these all together, we report that after cells' contraction highly compressed triangles are observed mostly in the region between the two cells, which correspond to highly densified regions of the network. These regions of high density have been observed experimentally [12, 23, 33]. In these experiments, the densification between contractile cells is due to aligned and densely packed matrix fibers being in tension, forming bands between the cells. Our simulations depict that highly tensile stretches occur entirely between the two cells and the fibers corresponding these stretches are aligned and oriented in the horizontal direction connecting the two cells, while the compressive stretches belong to fibers that are perpendicular to the tensile ones. Fibers in high tension form linear paths between the two cells, thereby the proposed model of fiber buckling captures that the band formation of densely packed and aligned fibers observed in experiments.

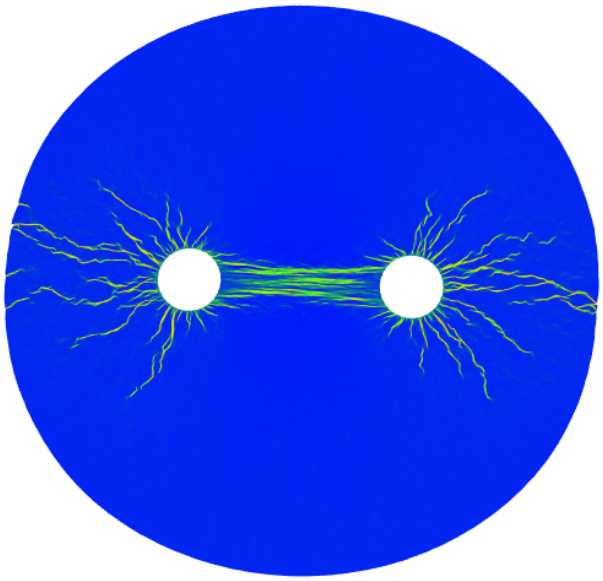

FIGURE 3.30. Band formation between two contractile cells in a network of resolution 100. The network is coloured based on the network's area density.

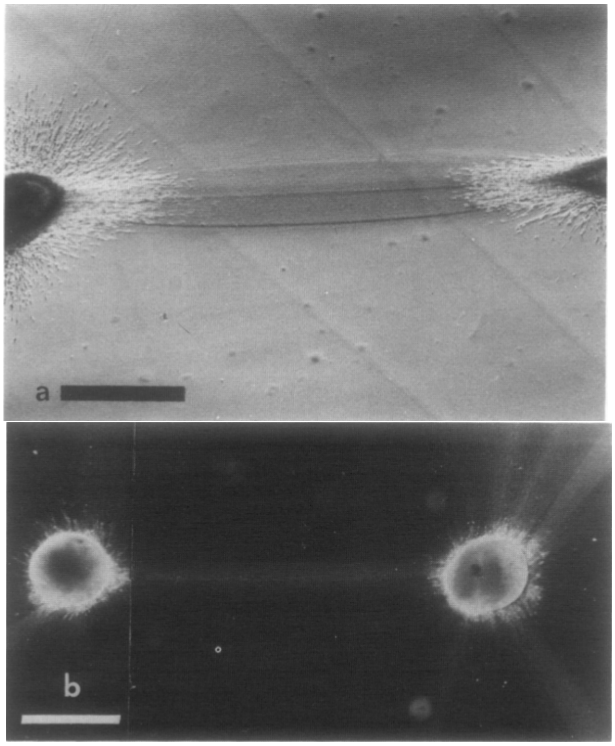

FIGURE 3.31. Band formation between two contracting cells, Stopak and Harris in [33].

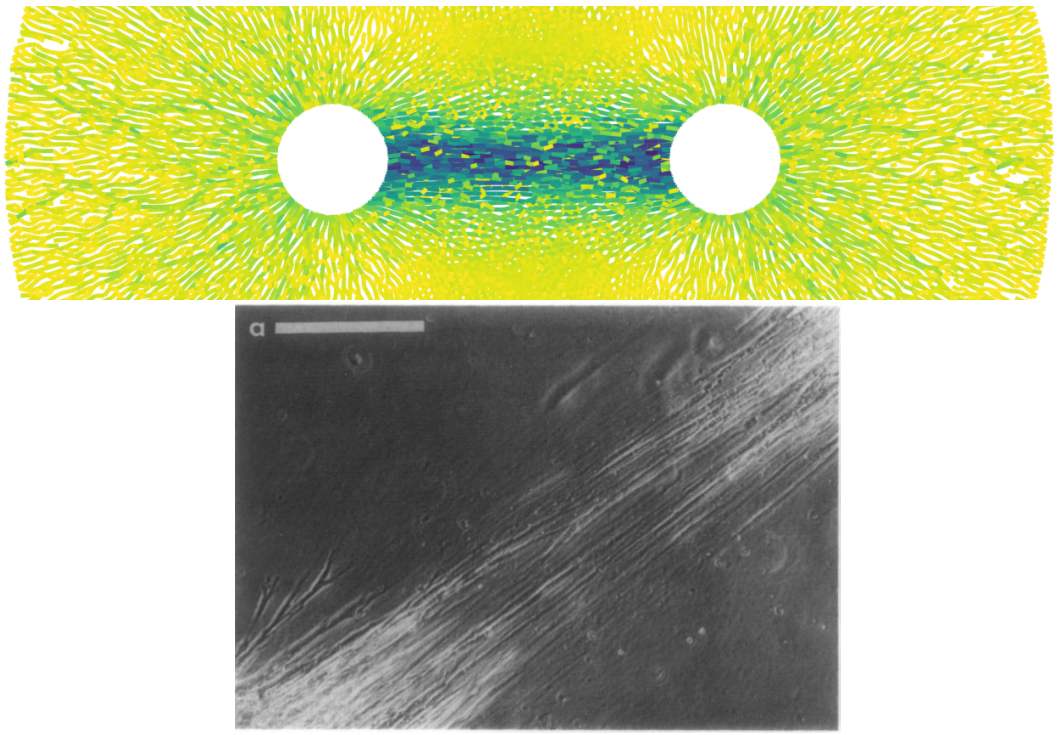

FIGURE 3.32. ***Up*:** Simulated tensile stretches. The band consists of densely packed and aligned fibers in high tension. ***Down*:** The band consists of aligned fibers under tension, Stopak and Harris in [33].

We saw previously, in both networks of the two resolutions, that displacements induced by the cells' contraction reach the boundary of the network. This is a result of how close the boundary is to the cells, as well as of the fact that the boundary is free of forces, i.e. its nodes are free to move. We note that these facts do not affect the interaction between them. In order to validate this, we constructed a network of bigger radius $A = 7a$, and repeat the simulations by keeping the initial distance between cells the same , $d = 4a$ and the outer boundary free to move. We present here the result for the network of 100 resolution:

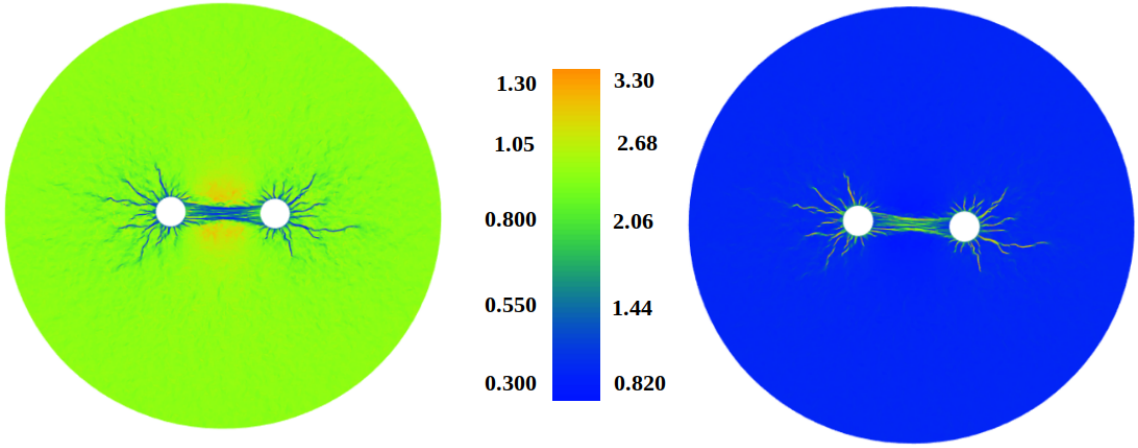

FIGURE 3.33. Network with bigger radius, $A = 7a$.

The band formation is not affected by how close the boundary of the domain is. Note that the magnitudes of $\mathscr{J}$ and density are very close to the respective magnitudes in the smaller network, Fig. (3.24).

CHAPTER 4

DISCUSSION

The discrete computational model presented in this study suggests that the nonlinear elastic behavior of the fibers contained in the Extracellular Matrix, characterized by strain stiffening when fibers are under tension and by buckling when fibers are being compressed facilitates the long range propagation of matrix displacements, which in turn promotes cellular mechanosensing. In order to quantify the simulated displacements induced by a contracting cell in the network, we fit the radial displacements $u(r)$ to distance r using the equations Ar^{-n}, $Ar^{-n}+Br^{n}$ proposed and used by Notbohm *et al.,* in [23] and Burkel and Notbohm in [4, 5] and in addition the equations $Ar^{-n_1}+Br^{n_2}$ and $Ar^{-n}+Br$, and reported the fitting parameter n. The fitting power n requires measuring only the field of displacements and not the field of stresses and quantifies the distance over which the displacement field propagates. For a fully connected network, with average number of fibers at each node $C \approx 6$, displacements decay with $u \sim r^{-0.56}$ much slower than predicted by classical linear theory, where $n = 1$ [23, 26]. The long range propagation of displacements in our networks agrees with previous experiments [4, 23, 37] where contracting cells were observed to produce displacement fields that propagated over a long range. For less connected networks, we report a decay power $n \approx 0.57$ for $C \approx 5$, $n \approx 0.35$ for networks with $C \approx 4$, and $n \approx 0.9$ for $C \approx 3$. These findings suggest that long range propagation is present in networks with lower connectivity, until a critical value is reached at which the induced displacements decay fast as they would in an elastic material. Thus, the critical value in our networks is $C \approx 3$, which comes in contrast to a previous two-dimensional model [23] suggesting that the critical connectivity is $C = 4$. This result is under investigation and we shall need to check additional aspects in order to validate it. For example, we observe that the displacements in the network of $C \approx 4$ are very sparse through the network, in contrast to the network of $C3$, where there are many nodes that remain in their initial positions, Fig. (3.22), thereby we

consider to simulate networks with intermediate connectivities and compare the resulting decay of displacements. In addition, in the network of $C \approx 3$ for which the displacements decay faster with $n \approx 0.9$ close to the elastic solution, we observed that compressive strains are almost absent, Fig. (3.17). This is a strong evidence that tension-stiffening in the absence of buckling cannot facilitate the slow displacement decay we reported in networks where the compressive strains were dominant. We conclude that the simulated buckling in our model results in cell-induced displacements that propagate over a longer range than predicted by linear elasticity.

In addition to the statements above, regarding the decay power of displacements, we report its dependence on cell's contraction level while previous studies, [23, 26], suggest there is no relation between how much the cell contracts and how far displacements propagate. This finding is also a result of the nonlinear relation in the force-stretch formula for fibers under compression we propose here instead of the linear one investigated by previous models.

We report an additional finding while observing the compressive and tensile strains of fibers in the deformed configurations fro each one of the networks. Apart from the critical connectivity $C \approx 3$, in the rest of the networks we see that tensed fibers are straightened generating chains that emanate radially from the contracting cell while the compressed fibers are oriented in the angular direction. This finding agrees with a recent experiment performed by Burkel in [4] where they additionally reported that compressed fibers oriented in the angular direction exhibit also prominent buckling:

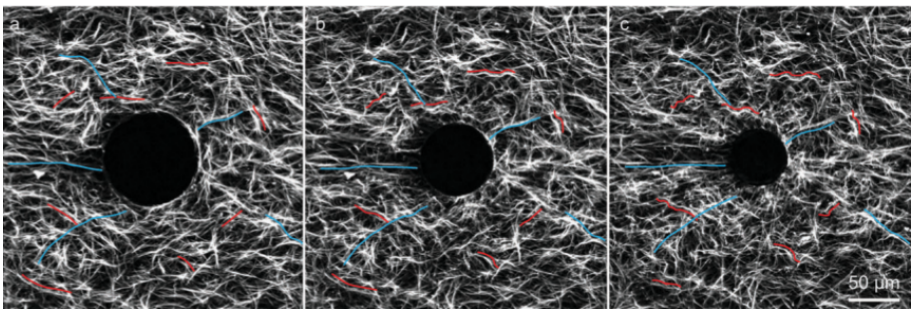

FIGURE 4.1. Burkel and Notbohm in [4]. Fiber buckling and straightening. Red lines show fibers oriented in the angular direction that buckle; blue lines show fibers oriented in the radial direction that straighten.

Finally, our simulations with two contractile cells reveal that the proposed compression-buckling and tension-stiffening of the fibers enable cells to induce displacements that result in the formation of linear tether-like bands between them. These bands have been reported to be formed by aligned and densely packed matrix fibers. Our simulations are able to capture this mechanism, with highly tensile strains to occur in the inter-cellular region and the compresive strains to localize perpendicular to the tensile fibers. Following we present the band formation

as predicted by the models with the linear relation of force-stretch, of Notbohm and Sopher in [23, 30] respectively:

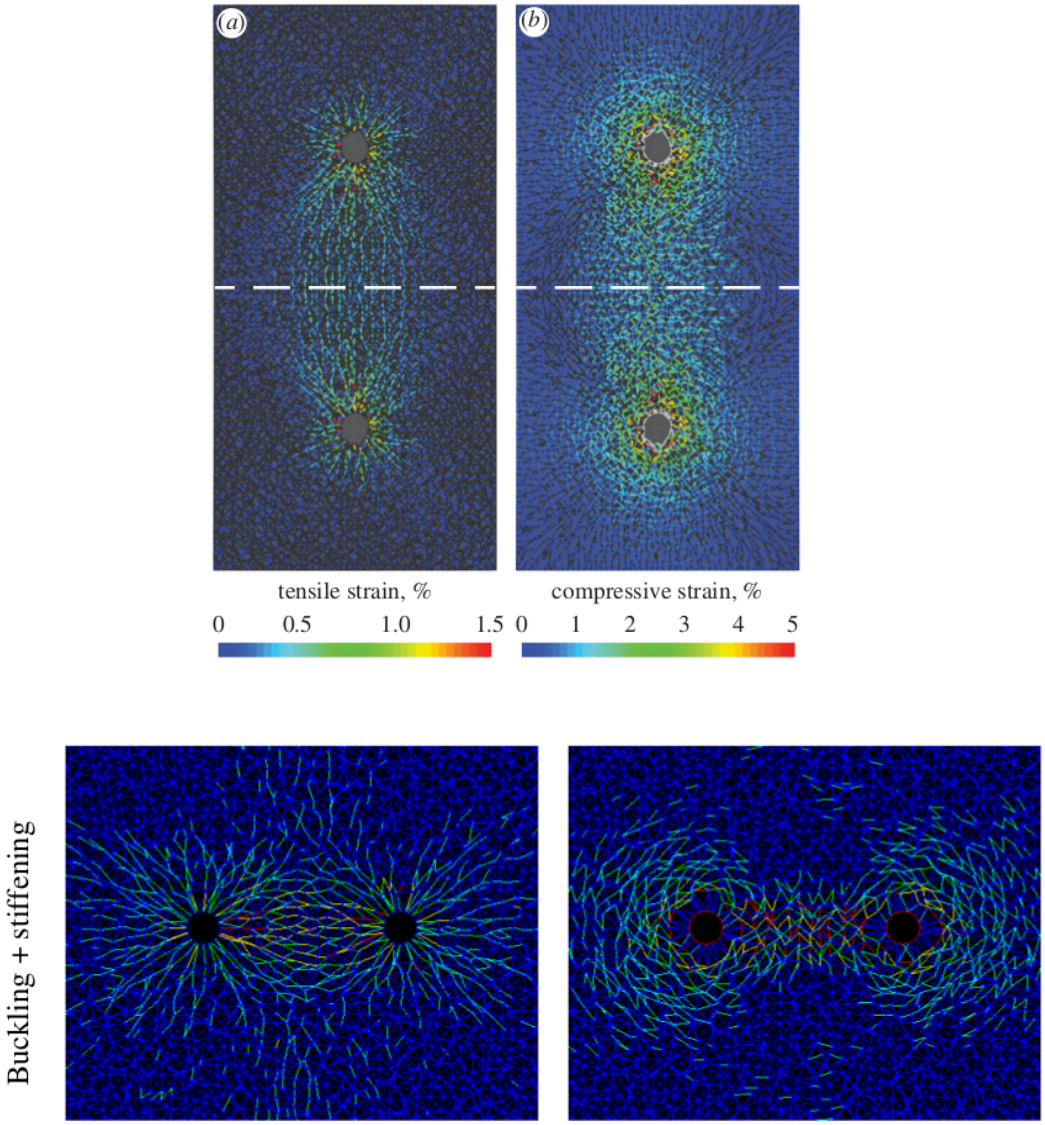

FIGURE 4.2. ***Up*:** Notbohm *et al.,* 2015 [23]. ***Down*:** Sopher *et al.,* [30]. Simulated tensile (left) and compressive (right) stretches.

We see that tensile stretches, in both of the above approaches, occur in the inter-cellular region but cannot depict the alignment of fibers with the same fidelity as our model, Fig. (3.30) and (3.32) on page (64). The localization of the band is not clearly depicted and the fiber alignment is not as apparent as in our simulations. In addition, both of them fail to capture the geometry of the tether. We observe here a broad region of tensile stretches, compared to our model where the band width of tensile fibers resembles the one observed in experiments, Fig. (3.32).

The proposed model is able to capture the two main concepts: the long range propagation of displacements in the Extracellular Matrix that enables cellular mechanosensing and the formation of tethers between cells that facilitates their communication. In addition, we report the dependence of the propagation of displacements on the level a cell contracts, a novel finding directly resulted from the nonlinear relation that models the fiber-buckling. Yet, there are still a lot to examine, let alone to discover, considering the complexity that these networks exhibit in biological tissues. Major challenges for future work include simulations with intermediate connectivities, in order to validate the critical connectivity for which the network resembles a linear elastic material. In addition, regarding networks with two contracting cells, an important feature is to let the cells free to move, after their contraction, and report their behaviour. And, finally, the extension of the model to three dimensions.

BIBLIOGRAPHY

[1] R. ABEYARATNE, *Lecture Notes on The Mechanics of Elastic Solids*, `http://web.mit.edu/abeyaratne/lecture_notes.html`, 2006.

[2] Y. BEATRICE, *Biology of the extracellular matrix: An overview*, (2014).

[3] A. BROWN, R. LITVINOV, D. DISCHER, P. PUROHIT, AND J. WEISEL, *Multiscale Mechanics of Fibrin Unfolding and Loss of Water*, Science, 741 (2009).

[4] B. BURKEL AND J. NOTBOHM, *Mechanical response of collagen networks to nonuniform microscale loads.* , Soft Matter, (2017).

[5] B. BURKEL, M. PROESTAKI, S. TYZNIK, AND J. NOTBOHM, *Heterogeneity and nonaffinity of cell-induced matrix displacements*, Physical review E, (2018).

[6] O. CHAUDHURI, S. H. PAREKH, AND D. A. FLETCHER, *Reversible stress softening of actin networks*, 445 (2007), pp. 20–22.

[7] M. W. CONKLIN, J. C. EICKHOFF, K. M. RICHING, C. A. PEHLKE, K. W. ELICEIRI, P. P. PROVENZANO, A. FRIEDL, AND P. J. KEELY, *Aligned Collagen Is a Prognostic Signature for Survival in Human Breast Carcinoma*, AJPA, 178 (2011), pp. 1221–1232.

[8] E. CONTI AND F. C. MACKINTOSH, *Cross-Linked Networks of Stiff Filaments Exhibit Negative Normal Stress*, (2009), pp. 1–4.

[9] A. J. ENGLER, S. SEN, H. L. SWEENEY, AND D. E. DISCHER, *Matrix Elasticity Directs Stem Cell Lineage Specification*, (2006), pp. 677–689.

[10] M. GURTIN, *An Introduction to Continuum Mechanics*, Mathematics in Science and Engineering, 1981.

[11] R. HALDAR, N. SIKDAR, AND T. K. MAJI, *Interpenetration in coordination polymers: structural diversities toward porous functional materials*, materialstoday, 18 (2015), pp. 97–116.

[12] A. HARRIS, D. STOPAK, AND P. WILD, *Fibroblast traction as a mechanism for collagen morphogenesis*, Nature, (1981).

[13] R. O. HYNES AND K. M. YAMADA, *Extracellular Matrix Biology*, Cold Spring Harbor Laboratory Press.

[14] D. E. INGBER, *Mechanical control of tissue morphogenesis during embryological development*, 266 (2006), pp. 255–266.

[15] P. A. JANMEY, M. E. M. C. CORMICK, S. RAMMENSEE, J. L. LEIGHT, P. C. GEORGES, AND F. C. M. A. C. KINTOSH, *Negative normal stress in semiflexible biopolymer gels*, 6 (2007), pp. 4–7.

[16] J.NOCEDAL AND S.WRIGHT, *Numerical Optimization*, Springer.

[17] K. E. KASZA, A. C. ROWAT, J. LIU, T. E. ANGELINI, C. P. BRANGWYNNE, G. H. KOENDERINK, AND D. A. WEITZ, *The cell as a material*.

[18] O. V. KIM, R. I. LITVINOV, J. W. WEISEL, AND M. S. ALBER, *Biomaterials Structural basis for the nonlinear mechanics of fi brin networks under compression*, Biomaterials, 35 (2014), pp. 6739–6749.

[19] M. LINDE-MEDINA AND R. MARCUCIO, *Living tissues are more than cell clusters : The extracellular matrix as a driving force in morphogenesis*, Progress in Biophysics and Molecular Biology, (2018), pp. 1–6.

[20] C. M. LO, H. B. WANG, M. DEMBO, AND Y. L. WANG, *Cell movement is guided by the rigidity of the substrate*, Biophysical Journal, 79 (2000), pp. 144–152.

[21] S. MUNSTER, L. M. JAWERTH, B. LESLIE, J. WEITZ, B. FABRY, AND D. WEITZ, *Strain history dependence of the nonlinear stress response of fibrin and collagen networks.* , PNAS, (2013).

[22] C. M. NELSON AND M. J. BISSELL, *Of Extracellular Matrix , Scaffolds , and Signaling : Tissue Architecture Regulates Development , Homeostasis , and Cancer*, (2006), pp. 287–311.

[23] J. NOTBOHM, A. LESMAN, P. ROSAKIS, D. A. TIRRELL, AND G. RAVICHANDRAN, *Microbuckling of fibrin provides a mechanism for cell mechanosensing*, Journal of The Royal Society Interface, 12 (2015).

[24] J. NOTBOHM, A. LESMAN, D. A. TIRRELL, AND G. RAVICHANDRAN, *Quantifying cell-induced matrix deformation in three dimensions based on imaging matrix fibers*, Integr. Biol., (2015).

[25] P. P. PROVENZANO, K. W. ELICEIRI, J. M. CAMPBELL, D. R. INMAN, J. G. WHITE, AND P. J. KEELY, *local invasion*, 16 (2006), pp. 1–15.

[26] P. ROSAKIS, J. NOTBOHM, AND G. RAVICHANDRAN, *A model for compression-weakening materials and the elastic fields due to contractile cells*, Journal of the Mechanics and Physics of Solids, (2015).

[27] T. ROZARIO AND D. W. DESIMONE, *The extracellular matrix in development and morphogenesis : A dynamic view*, Developmental Biology, 341 (2010), pp. 126–140.

[28] J. M. SAWYER, J. R. HARRELL, G. SHEMER, J. SULLIVAN-BROWN, M. ROH-JOHNSON, AND B. GOLDSTEIN, *Apical constriction : A cell shape change that can drive morphogenesis*, Developmental Biology, 341 (2010), pp. 5–19.

[29] Q. SHI, R. P. GHOSH, H. ENGELKE, C. H. RYCROFT, L. CASSEREAU, J. A. SETHIAN, V. M. WEAVER, AND J. T. LIPHARDT, *Rapid disorganization of mechanically interacting systems of mammary acini*, Proceedings of the National Academy of Sciences, 111 (2014), pp. 658–663.

[30] R. SOPHER, H. TOKASH, S. NATAN, M. SHARABI, O. SHELAH, O. TCHAICHEEYAN, AND A. LESMAN, *Nonlinear elasticity of the extracellular matrix fibers facilitates efficient inter-cellular mechanical communication*, Biophysical Journal, 115 (2018).

[31] R. M. STATICS, *Nonlinear elasticity in biological gels*, 435 (2005), pp. 0–3.

[32] J. STEINWACHS, C. METZNER, K. SKODZEK, N. LANG, I. THIEVESSEN, C. MARK, S. MÜNSTER, K. E. AIFANTIS, AND B. FABRY, *Three-dimensional force microscopy of cells in biopolymer networks*, (2015).

[33] D. STOPAK AND A. HARRIS, *Connective Tissue Morphogenesis by Fibroblast Traction*, Developmental Biology, (1981).

[34] D. VADER, A. KABLA, D. WEITZ, AND L. MAHADEVAN, *Strain-Induced Alignment in Collagen Gels*, 4 (2009).

[35] V. VOGEL AND M. SHEETZ, *Local force and geometry sensing regulate cell functions*, Nature Reviews Molecular Cell Biology, 7 (2006), pp. 265–275.

[36] Q. WEN AND P. A. JANMEY, *Effects of non-linearity on cell – ECM interactions*, Experimental Cell Research, 319 (2013), pp. 2481–2489.

[37] J. P. WINER, S. OAKE, AND P. A. JANMEY, *Non-linear elasticity of extracellular matrices enables contractile cells to communicate local position and orientation*, PLoS ONE, 4 (2009).